Energy estimates and numerical verification of the stabilized Domain Decomposition Finite Element/Finite Difference approach for

Cent. Eur. J. Math. • 11(4) • 2013 • 702-733
DOI: 10.2478/s11533-013-0202-3

VERSITA

Central European Journal of **Mathematics**

Energy estimates and numerical verification of the stabilized Domain Decomposition Finite Element/Finite Difference approach for time-dependent Maxwell's system

Research Article

Larisa Beilina[1]*

1 Department of Mathematical Sciences, Chalmers University of Technology and Gothenburg University, 42196 Gothenburg, Sweden

Received 11 June 2012; accepted 31 July 2012

Abstract: We rigorously derive energy estimates for the second order vector wave equation with gauge condition for the electric field with non-constant electric permittivity function. This equation is used in the stabilized Domain Decomposition Finite Element/Finite Difference approach for time-dependent Maxwell's system. Our numerical experiments illustrate efficiency of the modified hybrid scheme in two and three space dimensions when the method is applied for generation of backscattering data in the reconstruction of the electric permittivity function.

MSC: 65M06, 65M15, 65M60

Keywords: Maxwell's equation • Hybrid finite element/finite difference method • Energy estimates • Gauge condition • Stabilized finite element method

1. Introduction

The goal of this paper is to present a proof of the energy estimate for the second order stabilized time-dependent Maxwell's equation for the electric field. This equation is used in the Domain Decomposition Finite Element/Finite Difference method developed in [2]. We also present a modification of the hybrid method of [2] and illustrate the efficiency of the new method using several examples in two and three space dimensions. In our proof of the energy estimate we adopt the technique of [19], where the energy estimates were derived for a single hyperbolic equation. The main new element in our analysis is that we derive the energy estimate for the time-dependent Maxwell's equation for the electric field with Coulomb-type gauge condition in the presence of the first order absorbing boundary conditions [12].

* *E-mail: larisa@chalmers.se*

This estimate gives a bound of the electric field E through the initial data and the source function of these equations. Thus, the energy estimate is useful for analyzing the stability properties of the proposed hybrid scheme.

The FDTD method, or Yee scheme, was introduced in 1966 in [27]. It is still the most popular scheme for finding numerical solutions to time-dependent Maxwell's equations since it is simple and efficient for implementation. However, it can be applied only on structured meshes and suffers from the representation of the solution on curved boundaries [9]. On the other hand, finite element methods (FEMs) can be applied on unstructured meshes and handle complex boundaries of the computational domain. Hybrid FEMs/FDMs combine the advantages of both schemes by applying FEMs only on a small part of the computational domain, where local mesh refinement is needed, and the FDTD method everywhere else.

In [10, 25, 26] the first stable time domain hybrid method was developed, which combined the finite difference time domain method (FDTD) of [27] on the structured part of the mesh with tetrahedral edge elements on the unstructured part. Here FDTD is viewed as a finite element method with edge elements on a hexahedral mesh, where the $H(\text{curl})$-conforming discretization of the electric field is obtained. In [10, 25, 26], implicit time-stepping is required inside the finite element domain to obtain stability in time. Contrary to [10, 25, 26], a fully explicit domain decomposition approach for solutions to time-dependent Maxwell's system was proposed and numerically verified in [2]. This method uses the Yee scheme [27] on the structured part of the mesh and a stabilized formulation for Maxwell's system on the unstructured part of the mesh.

The main idea of the proposed modified domain decomposition FEM/FDM of this paper is the following: we decompose the computational domain Ω into two subregions, $\Omega = \Omega_{FEM} \cup \Omega_{FDM}$, where in Ω_{FEM} finite elements and in Ω_{FDM} finite differences are used. We also note that in our algorithm Ω_{FEM} lies strictly inside Ω_{FDM}, and thus corner singularities of the computational solution for Maxwell's system in Ω_{FEM} are excluded. We assume the magnetic permeability $\mu(x) = 1$ in the whole domain Ω. Next, we assume the dielectric permittivity $\varepsilon(x) \geq 0$ in Ω_{FEM}, and we use the finite element method to solve Maxwell's system there. We also assume that both domains, Ω_{FEM} and Ω_{FDM}, overlap in two layers of structured nodes, and in these nodes the dielectric permittivity $\varepsilon(x) = 1$ as well. However, in Ω_{FEM} the mesh can be purely unstructured, and thus, adaptive algorithms can be applied there.

In this work we assume that in Ω_{FDM} the dielectric permittivity $\varepsilon(x) = 1$ and we solve the usual system of wave equations with first order absorbing boundary conditions [12] at the exterior boundary of Ω_{FDM}. This assumption is the main new element of our modified domain decomposition method: now instead of solving Maxwell's equations in Ω_{FDM} using the Yee scheme, as it was done in [2], we can use the usual explicit second order FDTD method to solve the wave equation in Ω_{FDM}. This new element improves the stability of the whole hybrid FEM/FDM scheme of [2] in the overlapping regions, the interpolation procedure that computes values of the electric field for the Yee scheme from the nodal values of the finite element solution in the exchange procedure is not used anymore in the modified method of this paper.

Efficiency of the proposed modified method is evident for solutions of Coefficient Inverse Problems (CIPs). For the solutions of electromagnetic CIPs, many algorithms need to accurately generate backscattered data at the boundary of the computational domain in order to reconstruct the dielectric permittivity $\varepsilon(x)$ inside the medium. In this case the forward problems for PDEs are considered in the entire space $\mathbb{R}^3$, see for example [3–5, 18]. It is efficient to approximate the solution of these Cauchy problems via the solution of a boundary value problem in a bounded domain with $\varepsilon(x) = \mu(x) = 1$ in a neighborhood of the boundary of the computational domain, and with $\varepsilon(x) \neq \text{const}$, $\varepsilon(x) \geq 0$ in the rest of the domain. In this case the time-dependent Maxwell's equations reduce to a system of independent wave equations in the neighborhood of the computational domain, and usage of the hybrid technique is preferable to the efficient solution of CIPs with coefficients that have properties as described above.

The numerical implementation of the proposed domain decomposition method is as follows. We use the explicit finite difference method in Ω_{FDM} similar to the one used in [6]. However, for the finite element discretization of Maxwell's equations in Ω_{FEM} we use the node-based curl-curl formulation with the divergence free condition that is similar to [2]. The proposed domain decomposition method of this paper is unaffected by instabilities that can occur when the two methods are hybridized since under our assumptions our Maxwell's system transforms into the system of wave equations at the overlapping nodes between Ω_{FEM} and Ω_{FDM}.

It is known that edge elements are the most satisfactory from a theoretical point of view [20] since they automatically satisfy the divergence free condition. However, they are less attractive for time-dependent computations, since the solution of a linear system is required at every time iteration. In addition, in the case of triangular or tetrahedral edge elements, the entries of the diagonal matrix resulting from mass-lumping are not necessarily strictly positive [11];

therefore, explicit time-stepping cannot be used in general. In contrast, nodal elements naturally lead to a fully explicit scheme when mass-lumping is applied [11, 17]. However, numerical solutions to Maxwell's equations using nodal finite elements may contain spurious solutions [21, 23]; there are various techniques to remove them [14–16, 22, 23]. We eliminate the spurious solutions by adding the divergence condition to the time-dependent equation for the electric field, which removes them when a local mesh refinement is applied and material discontinuities are not too big [2]. Our numerical tests of Section 7 show that in the case of CIPs similar to ones of [5, 18], these spurious solutions will not appear.

In subsection 7.2, we present numerical verification of the proposed modified domain decomposition method for the solution to time-dependent Maxwell's system. Test 4 in this section is similar to the one performed in [5, 18]. The reason to do so is the following. In [5, 18] we presented the reconstruction of refractive indexes of abnormalities from experimental data. In these works, for the solution of the electromagnetic CIP, a simplified mathematical model with a single wave equation was used instead of the full Maxwell's system. Despite this discrepancy, the reconstruction of both locations and refractive indices of dielectrics obtained in [5] was highly accurate. In addition, using the adaptivity technique the shape of the dielectric abnormalities was also reconstructed accurately. This can be explained by the fact that the data immersing procedure of [5, 18] smoothed out the scattering data, and thus, enforced them to be good for the considered model of the wave equation. Our conclusion from the numerical test of subsection 7.2 with a plane wave is that all meaningful reflections from the abnormalities inside Ω_{FEM} are only from the one component of the electric field while the reflections from the other components are negligible. This test explains results of experiments performed in [5, 18] when physicists could measure only one component of the electric field. Because of that, in [5, 18] we approximated our model problem of Maxwell's equations with a single wave equation. Tests of Section 7 illustrate results of [5, 18] where in some experiments with the plane wave it is reasonable to approximate the full Maxwell's system with a single wave equation. However, in our future work we plan to apply the modified method presented in this paper for the solution of CIPs similar to ones in [5, 18], but for the full Maxwell's system, and compare results.

The outline of this work is as follows. In Section 2 we briefly recall Maxwell's equations and in Section 3 we present the mathematical model considered in this work. In Section 4 we derive the energy estimate. Then in Section 5 we present the finite element method: in subsection 5.1 the explicit scheme for the electric field is presented, the finite difference scheme is summarized in subsection 5.2, and the first order absorbing boundary conditions for this scheme are presented in subsection 5.3. Next, we formulate the modified hybrid FEM/FDM in Section 6. Finally, in Section 7 we present numerical examples that demonstrate the efficiency of our adaptive hybrid FEM/FDM solver.

2. Maxwell's equations

Let $\Omega \subset \mathbb{R}^3$ be a bounded domain with a piecewise smooth boundary $\partial\Omega$, and $T = \text{const} > 0$. Let $L^2(\Omega)$ be the space of square integrable functions in Ω. We define $\Omega_T = \Omega \times (0, T)$, and $\partial\Omega_T = \partial\Omega \times (0, T)$. We consider Maxwell's equations in an inhomogeneous isotropic medium in Ω_T:

$$\begin{aligned} \frac{\partial D}{\partial t} - \nabla \times H = -J, \qquad \frac{\partial B}{\partial t} + \nabla \times E = 0, \qquad & \text{in} \quad \Omega_T, \\ D = \varepsilon E, \qquad B = \mu H, & \\ E(x,0) = E_0(x), \qquad H(x,0) = H_0(x). & \end{aligned} \tag{1}$$

Here $E(x,t)$ and $H(x,t)$ are the electric and magnetic fields, whereas $D(x,t)$ and $B(x,t)$ are the electric and magnetic inductions, respectively. The dielectric permittivity, $\varepsilon(x) > 0$, and the magnetic permeability, $\mu(x) > 0$, together with the current density, $J(x,t) \in \mathbb{R}^3$, are given and assumed piecewise smooth. Moreover, the electric and magnetic inductions satisfy Gauss's law

$$\nabla \cdot D = \rho, \qquad \nabla \cdot B = 0, \qquad \text{in} \quad \Omega_T, \tag{2}$$

where $\rho(x,t)$ is a given charge density. Traditionally, perfectly conducting boundary conditions for (1)–(2) are the most popular ones:

$$n \times E = 0, \qquad H \cdot n = 0, \qquad \text{on} \quad \partial\Omega_T.$$

Here n denotes the outward normal on $\partial\Omega$.

However, our goal is to construct an efficient solver for the forward problem (1) in order to generate data at $\partial\Omega$ to solve Coefficient Inverse Problems. As mentioned above, in the case of CIPs, forward problems are usually Cauchy problems. Therefore, we need to approximate the solution of the Cauchy problem via the solution of a boundary value problem in a bounded domain. On the other hand, if $\varepsilon(x)$, $\mu(x) = \text{const} > 0$ in a neighborhood Ω' of $\partial\Omega$, as is often the case in CIPs, then it is well known that for $(x,t) \in \Omega' \times (0,T)$, (1) provides with independent vector wave equations

$$\varepsilon\mu\partial_t^2 E - \Delta E = -\mu j, \qquad \varepsilon\mu\partial_t^2 H - \Delta H = \nabla \times J, \tag{3}$$

where $j = \mu\partial J/\partial t$. When solving CIPs in real-life applications, such as subsurface imaging or detecting explosives, it is efficient to bound the domain of interest by an artificial boundary and impose absorbing boundary conditions. First order absorbing boundary conditions [12] work quite well for the case of a single hyperbolic PDE [3, 4] when the plane wave is initialized orthogonally to some part of the boundary $\partial\Omega$. Hence, by analogy, in this work we consider first order absorbing boundary conditions at $\partial\Omega_T$ for Maxwell's equations.

By eliminating B and D from (1) we obtain the following two independent second order systems of partial differential equations:

$$\begin{aligned} \varepsilon \frac{\partial^2 E}{\partial t^2} + \nabla \times (\mu^{-1} \nabla \times E) &= -j, \\ \mu \frac{\partial^2 H}{\partial t^2} + \nabla \times (\varepsilon^{-1} \nabla \times H) &= \nabla \times (\varepsilon^{-1} J), \end{aligned} \tag{4}$$

The initial conditions are

$$\begin{aligned} E(x,0) &= E_0(x), & \frac{\partial E}{\partial t}(x,0) &= \frac{\nabla \times H_0(x) - J(x,0)}{\varepsilon(x)}, \\ H(x,0) &= H_0(x), & \frac{\partial H}{\partial t}(x,0) &= -\frac{\nabla \times E_0}{\mu(x)}. \end{aligned}$$

3. Mathematical models

We are interested in the solution to equation (4) for the electric field with first order absorbing boundary conditions and appropriate initial conditions. For the above described setting of the problem it is convenient to use the domain decomposition finite element/finite difference method. In doing so we decompose Ω into two subregions, Ω_{FEM} and Ω_{FDM}, $\Omega = \Omega_{\text{FEM}} \cup \Omega_{\text{FDM}}$, see Figure 1. Ω_{FEM} corresponds to the domain where finite elements are used, and lies strictly inside Ω_{FDM}. In Ω_{FDM} we will use the finite difference method with first order absorbing boundary conditions.

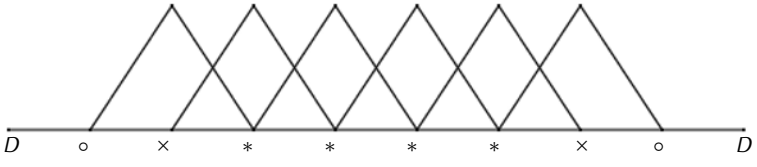

Figure 1. Domain decomposition between Ω_{FEM} and Ω_{FDM} in one dimension. The interior nodes of the unstructured finite element grid are denoted by stars, while circles and crosses denote nodes, which are shared between meshes in Ω_{FEM} and Ω_{FDM}. The circles are interior nodes ω_0 of the grid in Ω_{FDM}, while the crosses are interior nodes ω_x of the grid in Ω_{FEM}. At each time iteration, the solution obtained in Ω_{FDM} at ω_0 is copied to the corresponding nodes in Ω_{FEM}, while simultaneously the solution obtained in Ω_{FEM} at ω_x is copied to the corresponding nodes in Ω_{FDM}.

We also assume that we are working in a nonconducting medium, which means that the charge density $\rho = 0$. Our next assumption is that the magnetic permeability $\mu(x) = 1$, $x \in \Omega$, and we let the electric permittivity $\varepsilon(x)$ be such that

$$\begin{aligned} &\varepsilon(x) \geq 1, \qquad \text{for} \quad x \in \Omega_{\text{FEM}}, \qquad \varepsilon(x) \in C^2(\overline{\Omega}), \\ &\varepsilon(x) = 1, \qquad \text{for} \quad x \in \Omega_{\text{FDM}}. \end{aligned} \tag{5}$$

Let us formulate the model problem for the electric field E with first order absorbing boundary conditions [12] at the boundary $\partial\Omega$:

$$\begin{aligned} \varepsilon \frac{\partial^2 E}{\partial t^2} + \nabla \times (\nabla \times E) &= -j, && \text{in} \quad \Omega_T, \\ \nabla \cdot (\varepsilon E) &= 0, && \text{in} \quad \Omega_T, \\ E(x,0) = f_0(x), \qquad E_t(x,0) &= f_1(x), && \text{in} \quad \Omega, \\ \partial_n E(x,t) &= -\partial_t E(x,t), && \text{on} \quad \partial\Omega_T. \end{aligned} \tag{6}$$

Here we assume that

$$j \in L_2(\Omega_T), \qquad f_0 \in H^1(\Omega), \qquad f_1 \in L_2(\Omega).$$

As we have mentioned above, we will use the domain decomposition finite element/finite difference method for the numerical solution to (6). This means that for the solution to (6) in Ω_{FDM} we shall use the finite difference method on a structured mesh with constant coefficients $\varepsilon = \mu = 1$. As we have pointed out in Section 2, in this case problem (6) transforms to the system of vector wave equations (3).

In Ω_{FEM}, however, we shall use finite elements on a sequence of non-degenerate unstructured meshes $K_h = \{K\}$, with elements K consisting of triangles in $\mathbb{R}^2$ and tetrahedra in $\mathbb{R}^3$ [7]. Efficiency of the resulting domain decomposition FEM/FDM scheme in Ω is obtained by using the mass lumping in both space and time in Ω_{FEM}, which makes the scheme fully explicit [13]. In Ω_{FEM} we associate with K_h a (continuous) mesh function $h = h(x)$, which represents the diameter of the element $K \ni x$. For the time discretization we let $J_\tau = \{J\}$ be a partition of the time interval $I = [0, T]$, where $0 = t_0 < t_1 < \ldots < t_N = T$ is a sequence of discrete time steps with associated time intervals $J = (t_{k-1}, t_k]$ of constant length $\tau = t_k - t_{k-1}$. Below, for any vector function $u \in \mathbb{R}^3$ our notation $u \in L^2(\Omega)$ or $u \in H^k(\Omega)$, $k = 1, 2$, means that every component of the vector function u belongs to this space.

Keeping the above remark in mind, it is well known that when using standard, piecewise continuous $H^1(\Omega)$-conforming FE for the numerical solution to Maxwell's equations, we have the following difficulties. First, in general the solution to (4) lies in the space $H_0(\text{curl}, \Omega) \cap H(\text{div}, \Omega)$ with

$$H_0(\text{curl}, \Omega) = \left\{u \in L^2(\Omega) : \nabla \times u \in L^2(\Omega),\ u \times n = 0 \text{ on } \partial\Omega\right\}, \qquad H(\text{div}, \Omega) = \left\{u \in L^2(\Omega) : \nabla \cdot u \in L^2(\Omega)\right\},$$

where n is the unit outward normal to $\partial\Omega$. The space $H_0(\text{curl}, \Omega) \cap H(\text{div}, \Omega)$ is strictly larger than $H^1(\Omega)$ when Ω has re-entrant corners [20, p. 191]. However, this restriction is of no concern in our method, because we will use finite elements only in Ω_{FEM}, which lies strictly inside Ω; hence, in our case corner singularities are excluded. Second, because the bilinear form $a(u, v) = (\nabla \times u, \nabla \times v)$ is not coercive without some (at least weak) restriction to divergence-free functions, direct application of the finite element method to the numerical solution to Maxwell's equations using $H^1(\Omega)$-conforming nodal finite elements can result in spurious solutions (the finite element solution does not satisfy the divergence condition from (6)). To remove these spurious solutions from the finite element solution, we shall add a Coulomb-type gauge condition to enforce the divergence condition [1, 22, 23].

Thus, we modify equations (6) with $0 \leq s \leq 1$ to be

$$\varepsilon \frac{\partial^2 E}{\partial t^2} + \nabla \times (\nabla \times E) - s \nabla (\nabla \cdot (\varepsilon E)) = -j, \qquad \text{in} \quad \Omega_T, \tag{7}$$

$$E(x,0) = f_0(x), \qquad E_t(x,0) = f_1(x), \qquad \text{in} \quad \Omega, \tag{8}$$

$$\partial_n E(x,t) = -\partial_t E(x,t), \qquad \nabla \cdot E = 0, \qquad \text{on} \quad \partial\Omega_T, \tag{9}$$

$$\nabla \cdot E = 0 \quad \text{in} \quad \Omega' \subset \Omega_{\text{FDM}}, \qquad \varepsilon(x) = 1 \quad \text{in} \quad \Omega_{\text{FDM}}, \tag{10}$$

where the subdomain Ω' is a small neighborhood of the outer boundary $\partial\Omega$. We note that as soon as the term $-s\nabla(\nabla\cdot(\varepsilon E))$ is incorporated in equation (7), the first equation in (10) is an over-determination. On the other hand, this over-determination takes place only in a small neighborhood of the boundary $\partial\Omega$ rather than in the entire domain Ω. Likewise, we do not use (10) in our numerical experiments.

Since the modified bilinear form $a(u,v)=(\nabla\times u,\nabla\times v)+s(\nabla\cdot u,\nabla\cdot v)$ is now coercive on $H^1(\Omega)$ [24], problem (7)–(9) is now well posed. The addition of the term $s(\nabla\cdot u,\nabla\cdot v)$ does not change any solution to (7)–(9), but only provides a stabilization of the variational formulation, see also [20, p. 191].

Using Gauss's law (2), problem (7)–(9) can be rewritten as

$$\varepsilon\frac{\partial^2 E}{\partial t^2}+\nabla(\nabla\cdot E)-\nabla\cdot(\nabla E)-s\nabla(\nabla\cdot(\varepsilon E))=-j, \qquad \text{in} \quad \Omega_T, \tag{11}$$

$$E(x,0)=f_0(x), \qquad E_t(x,0)=f_1(x), \qquad \text{in} \quad \Omega, \tag{12}$$

$$\partial_n E(x,t)=-\partial_t E(x,t), \qquad \nabla\cdot E=0, \qquad \text{on} \quad \partial\Omega_T, \tag{13}$$

$$\nabla\cdot E=0 \quad \text{in} \quad \Omega'\subset\Omega_{\text{FDM}}, \qquad \varepsilon(x)=1 \quad \text{in} \quad \Omega_{\text{FDM}}. \tag{14}$$

4. Energy estimate for problem (11)–(14)

In this section we prove the uniqueness theorem, or energy estimate, for the vector $E\in H^2(\Omega_T)$ of equation (11)–(14), using the technique of [19], where the energy error estimates were derived for a single hyperbolic equation.

Theorem 4.1.
Assume that condition (5) on the coefficient $\varepsilon(x)$ holds. Let $\Omega\subset\mathbb{R}^3$ be a bounded domain with piecewise smooth boundary $\partial\Omega$. For any $t\in(0,T)$, let $\Omega_t=\Omega\times(0,t)$. Suppose there exists a solution $E\in H^2(\Omega_T)$ of (11)–(14). Then the vector E is unique and there exists a constant $B=B(\|\varepsilon\|_\Omega,t,s)$ depending only on $\|\varepsilon\|_\Omega$, t and $0\le s\le 1$ such that the following energy estimate is true for all $\varepsilon\ge 1$ in (11)–(14):

$$\|\sqrt{\varepsilon}\,\partial_t E(x,t)\|^2_{L_2(\Omega)}+\|\nabla E(x,t)\|^2_{L_2(\Omega)}+\|\sqrt{s\varepsilon-1}\,\nabla\cdot E(x,t)\|^2_{L_2(\Omega)}$$
$$\le B\left[\|j\|^2_{L_2(\Omega_t)}+\|\sqrt{\varepsilon}\,f_1\|^2_{L_2(\Omega)}+\|\nabla f_0\|^2_{L_2(\Omega)}+\|f_0\|^2_{L_2(\Omega)}+\|\sqrt{s\varepsilon-1}\,\nabla\cdot f_0\|^2_{L_2(\Omega)}\right].$$

Proof. First we multiply the first equation of (11)–(14) by $2\partial_t E$ and integrate over $\Omega\times(0,t)$ to get

$$\int_0^t\int_\Omega 2\varepsilon\partial_{tt}E\,\partial_t E\,dx\,d\tau+\int_0^t\int_\Omega 2\nabla(\nabla\cdot E)\partial_t E\,dx\,d\tau-\int_0^t\int_\Omega 2\nabla\cdot(\nabla E)\partial_t E\,dx\,d\tau$$
$$-s\int_0^t\int_\Omega 2\nabla(\nabla\cdot(\varepsilon E))\partial_t E\,dx\,d\tau=-2\int_0^t\int_\Omega j\partial_t E\,dx\,d\tau. \tag{15}$$

Integrating the first term of (15) in time we get

$$\int_0^t\int_\Omega\partial_t(\varepsilon\partial_t E^2)\,dx\,d\tau=\int_\Omega(\varepsilon\partial_t E^2)(x,t)\,dx-\int_\Omega\varepsilon f_1^2(x,t)\,dx. \tag{16}$$

Integrating the second term of (15), which corresponds to the divergence, by parts in space we have

$$2\int_0^t\int_\Omega\nabla(\nabla\cdot E)\partial_t E\,dx\,d\tau=2\int_0^t\int_{\partial\Omega}\partial_t E\,n\cdot(\nabla\cdot E)\,dS\,d\tau-2\int_0^t\int_\Omega(\nabla\cdot E)(\nabla\cdot\partial_t E)\,dx\,d\tau$$
$$=2\int_0^t\int_{\partial\Omega}\partial_t E\,n\cdot(\nabla\cdot E)\,dS\,d\tau-\int_0^t\int_\Omega\partial_t(\nabla\cdot E)^2\,dx\,d\tau. \tag{17}$$

The term $2\int_0^t\int_{\partial\Omega}\partial_t E\, n\cdot(\nabla\cdot E)\,dS\,d\tau = 0$, since by (14), $\nabla\cdot E = 0$ in a small neighborhood of $\partial\Omega$. Next, integrating the last term of (17) in time and using (12) we have

$$-\int_0^t\int_\Omega \partial_t(\nabla\cdot E)^2\,dx\,d\tau = -\int_\Omega(\nabla\cdot E)^2(x,t)\,dx + \int_\Omega(\nabla\cdot E)^2(x,0)\,dx = -\int_\Omega(\nabla\cdot E)^2(x,t)\,dx + \int_\Omega(\nabla\cdot f_0)^2(x)\,dx. \quad (18)$$

Integrating the third term of (15), which corresponds to the gradient, by parts in space and using (12) we get

$$\begin{aligned} 2\int_0^t\int_\Omega \nabla\cdot(\nabla E)\,\partial_t E\,dx\,d\tau &= 2\int_0^t\int_{\partial\Omega}(\partial_t E)\,\partial_n E\,dS\,d\tau - 2\int_0^t\int_\Omega(\nabla E)(\nabla\partial_t E)\,dx\,d\tau \\ &= -2\int_0^t\int_{\partial\Omega}(\partial_t E)^2\,dS\,d\tau - \int_0^t\int_\Omega \partial_t|\nabla E|^2\,dx\,d\tau. \end{aligned} \quad (19)$$

Integrating the last term of (19) in time and using (12) we obtain

$$-\int_0^t\int_\Omega \partial_t|\nabla E|^2\,dx\,d\tau = -\int_\Omega|\nabla E|^2(x,t)\,dx + \int_\Omega|\nabla E|^2(x,0)\,dx = -\int_\Omega|\nabla E|^2(x,t)\,dx + \int_\Omega|\nabla f_0|^2(x)\,dx. \quad (20)$$

Integrating the augmented term of (15) in space we have

$$\begin{aligned} 2s\int_0^t\int_\Omega \nabla(\nabla\cdot(\varepsilon E))\,\partial_t E\,dx\,d\tau &= 2s\int_0^t\int_{\partial\Omega}\partial_t E\,n\cdot(\nabla\cdot(\varepsilon E))\,dS\,d\tau - 2s\int_0^t\int_\Omega(\nabla\cdot(\varepsilon E))(\nabla\cdot\partial_t E)\,dx\,d\tau \\ &= 2s\int_0^t\int_{\partial\Omega}\partial_t E\,n\cdot(\nabla\cdot(\varepsilon E))\,dS\,d\tau - 2s\int_0^t\int_\Omega(\nabla\varepsilon\cdot E)\,\nabla\cdot(\partial_t E)\,dx\,d\tau \\ &\quad - s\int_0^t\int_\Omega \varepsilon\partial_t(\nabla\cdot E)^2\,dx\,d\tau. \end{aligned} \quad (21)$$

The term $2s\int_0^t\int_{\partial\Omega}\partial_t E\,n\cdot(\nabla\cdot(\varepsilon E))\,dS\,d\tau = 0$, since $\varepsilon = 1$ on the boundary $\partial\Omega$, and by (14), $\nabla\cdot E = 0$ on a small neighborhood of $\partial\Omega$. Next, integrating in space one more time the term $2s\int_0^t\int_\Omega(\nabla\varepsilon\cdot E)\,\nabla\cdot(\partial_t E)\,dx\,d\tau$ in (21) we have

$$\begin{aligned} -2s\int_0^t\int_\Omega(\nabla\varepsilon\cdot E)\,\nabla\cdot(\partial_t E)\,dx\,d\tau &= -2s\int_0^t\int_{\partial\Omega}(\nabla\varepsilon\cdot E)\,n\cdot(\partial_t E)\,dx\,d\tau + 2s\int_0^t\int_\Omega\nabla(\nabla\varepsilon\cdot E)(\partial_t E)\,dx\,d\tau \\ &= 2s\int_0^t\int_\Omega\nabla(\nabla\varepsilon\cdot E)\,\partial_t E\,dx\,d\tau. \end{aligned}$$

Here, the integral $-2s\int_0^t\int_{\partial\Omega}(\nabla\varepsilon\cdot E)\,n\cdot(\partial_t E)\,dx\,d\tau = 0$, since $\varepsilon = 1$ in a small neighborhood of $\partial\Omega$ and hence $\nabla\varepsilon = 0$ in this neighborhood. Next, collecting the estimates (16)–(21), (27), using the fact that $2\int_0^t\int_{\partial\Omega}(\partial_t E)^2\,dS\,d\tau \geq 0$ and substituting them in (15), we get

$$\begin{aligned} &\int_\Omega(\varepsilon\partial_t E^2)(x,t)\,dx - \int_\Omega(\nabla\cdot E)^2(x,t)\,dx + \int_\Omega|\nabla E|^2(x,t)\,dx + s\int_0^t\int_\Omega\varepsilon\partial_t(\nabla\cdot E)^2\,dx\,d\tau \\ &\quad\leq 2\int_0^t\int_\Omega|j||\partial_t E|\,dx\,d\tau + \int_\Omega\varepsilon f_1^2(x,t)\,dx - \int_\Omega(\nabla\cdot f_0)^2(x)\,dx + \int_\Omega|\nabla f_0|^2(x)\,dx \\ &\qquad + 2s\int_0^t\int_\Omega|\nabla(\nabla\varepsilon\cdot E)||\partial_t E|\,dx\,d\tau. \end{aligned} \quad (22)$$

Let $A = A(\|\varepsilon\|_{C^2(\Omega)}, s) > 0$ denote the constant depending only on $\|\varepsilon\|_\Omega$, t, and s. Now we can write the estimate

$$|\nabla(\nabla\varepsilon \cdot E)| \le A(|E| + |\nabla E|).$$

Using the above and the inequality $2ab \le a^2 + b^2$, we estimate the last term in (22) as

$$2s \int_0^t \int_\Omega |\nabla(\nabla\varepsilon \cdot E)| |\partial_t E| \, dx \, d\tau \le 2sA \int_0^t \int_\Omega |\partial_t E| \cdot (|E| + |\nabla E|) \, dx \, d\tau. \tag{23}$$

With another constant A we have

$$2s \int_0^t \int_\Omega |\nabla(\nabla\varepsilon \cdot E)| |\partial_t E| \, dx \, d\tau \le A \int_0^t \int_\Omega |\partial_t E|^2 \, dx \, d\tau + A \int_0^t \int_\Omega (|E| + |\nabla E|)^2 \, dx \, d\tau.$$

The second integral in the right hand side of (23) can be estimated as

$$A \int_0^t \int_\Omega (|E| + |\nabla E|)^2 \, dx \, d\tau \le 2A \int_0^t \int_\Omega |E|^2 \, dx \, d\tau + 2A \int_0^t \int_\Omega |\nabla E|^2 \, dx \, d\tau. \tag{24}$$

Let us estimate the term $\int_0^t \int_\Omega |E|^2 \, dx \, d\tau$ in (24). First we make the transformation

$$E(x,t) = E(x,0) + \int_0^t \partial_t E \, dx \, d\tau. \tag{25}$$

Taking the square of (25), integrating the result in space and using the estimate $(a+b)^2 \le 2a^2 + 2b^2$, we get

$$\int_\Omega |E|^2 \, dx \le 2 \int_\Omega |E|^2(x,0) \, dx + 2 \int_\Omega \left(\int_0^t |\partial_t E| \, d\tau \right)^2 dx \le 2 \int_\Omega |E|^2(x,0) \, dx + 2t \int_0^t \int_\Omega |\partial_t E|^2 \, d\tau \, dx.$$

Using the initial condition (12) we have

$$\int_\Omega |E|^2 \, dx \le 2\|f_0\|^2_{L_2(\Omega)} + 2t \int_0^t \int_\Omega |\partial_t E|^2 d\tau \, dx.$$

Integrating the above equation in the time interval $(0, t)$, we get

$$\int_0^t \int_\Omega |E|^2 \, dx \, d\tau \le 2t\|f_0\|^2_{L_2(\Omega)} + 2t^2 \int_0^t \int_\Omega |\partial_t E|^2 \, d\tau \, dx.$$

Substituting the above expression in (23) and using (24) with the constant $B = B(\|\varepsilon\|_{C^2(\Omega)}, t, s) > 0$, we get

$$\begin{aligned} A \int_0^t \int_\Omega (|\partial_t E|^2 + |\nabla E|^2) \, dx \, d\tau &\le 2A \left(2t\|f_0\|^2_{L_2(\Omega)} + 2t^2 \int_0^t \int_\Omega |\partial_t E|^2 \, d\tau \, dx \right) + 2A \int_0^t \int_\Omega |\nabla E|^2 \, dx \, d\tau \\ &\le B \int_0^t \int_\Omega (|\partial_t E|^2 + |\nabla E|^2) \, dx \, d\tau + B \int_\Omega f_0^2 \, dx, \end{aligned}$$

and thus we get the following estimate for the augmented term in (22):

$$2s\int_0^t\int_\Omega |\nabla(\nabla\varepsilon\cdot E)||\partial_t E|\,dx\,d\tau \le A\int_0^t\int_\Omega (|\partial_t E|^2+|\nabla E|^2)\,dx\,d\tau + A\int_\Omega f_0^2\,dx. \tag{26}$$

Now we estimate the remaining terms in (22). Integrating the fourth term of (22) in time we get

$$\begin{aligned} s\int_0^t\int_\Omega \varepsilon\partial_t(\nabla\cdot E)^2\,dx\,d\tau &= s\int_\Omega \varepsilon(\nabla\cdot E)^2(x,t)\,dx - s\int_\Omega \varepsilon(\nabla\cdot E)^2(x,0)\,dx \\ &= s\int_\Omega \varepsilon(\nabla\cdot E)^2(x,t)\,dx - s\int_\Omega \varepsilon(\nabla\cdot f_0)^2(x)\,dx. \end{aligned} \tag{27}$$

Finally, to estimate the first term in the right hand side of (22) we use the arithmetic-geometric mean inequality $2ab \le a^2+b^2$ to obtain

$$2\int_0^t\int_\Omega |j|\cdot|\partial_t E|\,dx\,d\tau \le \int_0^t\int_\Omega |j|^2\,dx\,d\tau + \int_0^t\int_\Omega |\partial_t E|^2\,dx\,d\tau. \tag{28}$$

Note that, by (5), for all ε such that $s\varepsilon \ge 1$ we have

$$B\int_0^t\int_\Omega (|\partial_t E|^2+|\nabla E|^2)\,dx\,d\tau \le B\int_0^t\int_\Omega \Big(\varepsilon|\partial_t E|^2+(s\varepsilon-1)(\nabla\cdot E)^2+|\nabla E|^2\Big)\,dx\,d\tau.$$

Substituting (26)–(28) into (22), we have the following estimate for all s such that $s\varepsilon-1\ge 0$:

$$\begin{aligned} \int_\Omega \Big(\varepsilon\partial_t E^2+|\nabla E|^2+(s\varepsilon-1)(\nabla\cdot E)^2\Big)(x,t)\,dx &\le \int_0^t\int_\Omega |j|^2\,dx\,d\tau \\ + B\int_0^t\int_\Omega \Big(\varepsilon|\partial_t E|^2+(s\varepsilon-1)(\nabla\cdot E)^2+|\nabla E|^2\Big)\,dx\,d\tau &+ \int_\Omega \Big(\varepsilon f_1^2+|\nabla f_0|^2+(s\varepsilon-1)(\nabla\cdot f_0)^2+Bf_0^2\Big)(x,t)\,dx. \end{aligned} \tag{29}$$

Let us denote

$$F(t) = \int_\Omega \Big(\varepsilon\partial_t E^2+|\nabla E|^2+(s\varepsilon-1)(\nabla\cdot E)^2\Big)(x,t)\,dx.$$

Then we can rewrite estimate (29) in the form

$$F(t) \le B\int_0^t F(\tau)\,d\tau + g(t), \tag{30}$$

where $g(t) = \int_0^t\int_\Omega |j|^2\,dx\,d\tau + \int_\Omega \big(\varepsilon f_1^2+|\nabla f_0|^2+(s\varepsilon-1)(\nabla\cdot f_0)^2+Af_0^2\big)(x,t)\,dx$. Applying Gronwall's inequality to (30) with a different constant B we get the desired estimate for all s such that $s\varepsilon\ge 1$:

$$\begin{aligned} &\int_\Omega \Big(\varepsilon\partial_t E^2+|\nabla E|^2+(s\varepsilon-1)(\nabla\cdot E)^2\Big)(x,t)\,dx \\ &\qquad\le B\left(\int_0^t\int_\Omega |j|^2\,dx\,d\tau + \int_\Omega \Big(\varepsilon f_1^2+|\nabla f_0|^2+(s\varepsilon-1)(\nabla\cdot f_0)^2+f_0^2\Big)(x,t)\,dx\right). \end{aligned}$$

□

5. The finite element method

We will formulate the finite element method for problem (7)–(9) with $f_0 = f_1 = 0$, which can be written as

$$\varepsilon \frac{\partial^2 E}{\partial t^2} + \nabla(\nabla \cdot E) - \nabla \cdot (\nabla E) - s\nabla(\nabla \cdot (\varepsilon E)) = -j, \qquad \text{in} \quad \Omega_T, \tag{31}$$

$$E(x,0) = 0, \qquad E_t(x,0) = 0, \qquad \text{in} \quad \Omega, \tag{32}$$

$$\partial_n E(x,t) = -\partial_t E(x,t), \qquad \text{on} \quad \partial\Omega_T, \tag{33}$$

$$\nabla \cdot E = 0, \qquad \text{on} \quad \partial\Omega_T,$$

$$\nabla \cdot E = 0 \quad \text{in} \quad \Omega' \subset \Omega_{\text{FDM}}, \qquad \varepsilon(x) = 1 \quad \text{in} \quad \Omega_{\text{FDM}}.$$

First we introduce the finite element trial space W_h^E for every component of the electric field E defined by

$$W_h^E = \left\{ w \in W^E : w\restriction_{K\times J} \in P_1(K) \times P_1(J),\ K \in K_h,\ J \in J_\tau \right\},$$

where $P_1(K)$ and $P_1(J)$ denote the set of linear functions on K and J, respectively, and

$$W^E = \left\{ w \in H^1(\Omega) \times I : w(\cdot, 0) = 0,\ \partial_n w\restriction_{\partial\Omega} = -\partial_t w \right\}.$$

We also introduce the finite element test space W_h^φ defined by

$$W_h^\varphi = \left\{ w \in W^\varphi : w\restriction_{K\times J} \in P_1(K) \times P_1(J),\ K \in K_h,\ J \in J_\tau \right\},$$

where

$$W^\varphi = \left\{ w \in H^1(\Omega) \times I : w(\cdot, T) = 0,\ \partial_n w\restriction_{\partial\Omega} = -\partial_t w \right\}.$$

Hence, the finite element spaces W_h^E and W_h^φ consist of continuous piecewise linear functions in space and time, which satisfy certain homogeneous initial and first order absorbing boundary conditions. We also define the following L_2 inner products and norms:

$$((p,q)) = \int_\Omega \int_0^T pq \, dx \, dt, \qquad \|p\|^2 = ((p,p)), \qquad (\alpha,\beta) = \int_\Omega \alpha\beta \, dx, \qquad |\alpha|^2 = (\alpha,\alpha).$$

The finite element method for (11)–(14) reads: Find $E \in W_h^E$ such that for all $\overline{\varphi} \in W_h^\varphi$,

$$-\left(\left(\varepsilon \frac{\partial E^k}{\partial t}, \frac{\partial \overline{\varphi}}{\partial t} \right) \right) - ((\nabla \cdot E^k, \nabla \cdot \overline{\varphi})) + ((\partial_t E^k, \overline{\varphi}))_{\partial\Omega} + ((\nabla E^k, \nabla \overline{\varphi})) + s\left((\nabla \cdot (\varepsilon E^k), \nabla \cdot \overline{\varphi}) \right) + ((j^k, \overline{\varphi})) = 0. \tag{34}$$

Here, the initial condition $(\partial E/\partial t)(x,0) = 0$ is imposed weakly through the variational formulation.

5.1. The explicit scheme for the electric field

We expand $E(x,t)$ in terms of the standard continuous piecewise linear functions $\{\varphi_i\}_{i=1}^M$ in space and $\{\psi_k\}_{k=1}^N$ in time as $E(x,t) = \sum_{k=1}^N \sum_{i=1}^M E_h \varphi_i(x)\psi_k(t)$, where $E_h = E_{h_{i,k}}$ denote unknown coefficients, substitute this expansion in variational formulation (34) with $\overline{\varphi}(x,t) = \varphi_j(x)\psi_l(t)$ and obtain the following system of discrete equations:

$$
\begin{aligned}
&- \sum_{K\in\Omega_{\mathrm{FEM}}} \sum_{k,l=1}^{N} \sum_{i,j=1}^{M} E_h \int_K \varepsilon(x)\varphi_i(x)\varphi_j(x) \int_{t_{k-1}}^{t_{k+1}} \partial_t\psi_k(t)\,\partial_t\psi_l(t)\,dx\,dt \\
&- \sum_{K\in\Omega_{\mathrm{FEM}}} \sum_{k,l=1}^{N} \sum_{i,j=1}^{M} E_h \int_K \nabla\cdot\varphi_i(x)\nabla\cdot\varphi_j(x) \int_{t_{k-1}}^{t_{k+1}} \psi_k(t)\psi_l(t)\,dx\,dt \\
&+ \sum_{\partial K\in\partial\Omega_{\mathrm{FEM}}} \sum_{k,l=1}^{N} \sum_{i,j=1}^{M} E_h \int_{\partial K} \varphi_i(x)\varphi_j(x) \int_{t_{k-1}}^{t_{k+1}} \partial_t\psi_k(t)\psi_l(t)\,dS\,dt \\
&+ \sum_{K\in\Omega_{\mathrm{FEM}}} \sum_{k,l=1}^{N} \sum_{i,j=1}^{M} E_h \int_K \nabla\varphi_i(x)\nabla\varphi_j(x) \int_{t_{k-1}}^{t_{k+1}} \psi_k(t)\psi_l(t)\,dx\,dt \\
&+ s \sum_{K\in\Omega_{\mathrm{FEM}}} \sum_{k,l=1}^{N} \sum_{i,j=1}^{M} E_h \int_K \nabla\cdot(\varepsilon\varphi_i(x))\nabla\cdot\varphi_j(x) \int_{t_{k-1}}^{t_{k+1}} \psi_k(t)\psi_l(t)\,dx\,dt \\
&+ \sum_{K\in\Omega_{\mathrm{FEM}}} \sum_{l=1}^{N} \sum_{j=1}^{M} \int_K \int_{t_{k-1}}^{t_{k+1}} j(x)\varphi_j(x)\psi_l(t)\,dx\,dt = I_1 + I_2 + I_3 + I_4 + I_5 + I_6 = 0.
\end{aligned}
\tag{35}
$$

Next, we compute explicitly the time integrals of (35) using the definition of piecewise linear functions in time, and get the following linear system of equations:

$$
\begin{aligned}
M\left(\mathbf{E}^{k+1} - 2\mathbf{E}^{k} + \mathbf{E}^{k-1}\right) = &-\tau^2 F^k + \tau^2 D\left(\frac{1}{6}\mathbf{E}^{k-1} + \frac{2}{3}\mathbf{E}^{k} + \frac{1}{6}\mathbf{E}^{k+1}\right) - \tau^2 G\left(\frac{1}{6}\mathbf{E}^{k-1} + \frac{2}{3}\mathbf{E}^{k} + \frac{1}{6}\mathbf{E}^{k+1}\right) \\
&- s\tau^2 C\left(\frac{1}{6}\mathbf{E}^{k-1} + \frac{2}{3}\mathbf{E}^{k} + \frac{1}{6}\mathbf{E}^{k+1}\right) + \frac{1}{2}\tau M_{\partial\Omega}(\mathbf{E}^{k+1} - \mathbf{E}^{k-1}),
\end{aligned}
\tag{36}
$$

with initial conditions $\mathbf{E}^0$ and $\mathbf{E}^1$ set to zero because of (32). Here, M and $M_{\partial\Omega}$ are the block mass matrices in space, D and C are the block stiffness matrices corresponding to the divergence terms, G is the stiffness matrix corresponding to the gradient term, F^k is the load vector at time level t_k corresponding to $j(\cdot,\cdot)$, whereas $\mathbf{E}^k$ denotes the nodal values of $E(\cdot,t_k)$.

For example, to compute explicitly the time integrals $\sum_{k,l=1}^{N}\int_{t_{k-1}}^{t_{k+1}}\partial_t\psi_k(t)\psi_l(t)\,dt$ in term I_3, we use the definition of piecewise linear functions in time and observe that all terms in $\sum_{k,l=1}^{N}\int_{t_{k-1}}^{t_{k+1}}\partial_t\psi_k(t)\psi_l(t)\,dt$ are zeros unless $l=k-1$, $l=k$, $l=k+1$. Thus we only have to compute the integrals

$$
\int_{t_{k-1}}^{t_{k+1}} \partial_t\psi_{k-1}\psi_k\,dt, \qquad \int_{t_{k-1}}^{t_{k+1}} \partial_t\psi_{k+1}\psi_k\,dt, \qquad \int_{t_{k-1}}^{t_{k+1}} \partial_t\psi_k\psi_k\,dt.
$$

To do that we have

$$
\begin{aligned}
\int_{t_{k-1}}^{t_{k+1}} \partial_t\psi_{k-1}\psi_k\,dt &= \int_{t_{k-1}}^{t_k} \partial_t\psi_{k-1}\psi_k\,dt + \int_{t_k}^{t_{k+1}} \partial_t\psi_{k-1}\psi_k\,dt = \int_{t_{k-1}}^{t_k} \partial_t\psi_{k-1}\psi_k\,dt = -\frac{1}{\tau}\int_{t_{k-1}}^{t_k} \frac{t-t_{k-1}}{t_k-t_{k-1}}\,dt = -\frac{1}{2}, \\
\int_{t_{k-1}}^{t_{k+1}} \partial_t\psi_{k+1}\psi_l\,dt &= \int_{t_{k-1}}^{t_k} \partial_t\psi_{k+1}\psi_k\,dt + \int_{t_k}^{t_{k+1}} \partial_t\psi_{k+1}\psi_k\,dt = \int_{t_k}^{t_{k+1}} \partial_t\psi_{k+1}\psi_k\,dt = -\frac{1}{\tau}\int_{t_k}^{t_{k+1}} \frac{t_{k+1}-t}{t_{k+1}-t_k}\,dt = \frac{1}{2}, \\
\int_{t_{k-1}}^{t_{k+1}} \partial_t\psi_k\psi_k\,dt &= \int_{t_{k-1}}^{t_k} \partial_t\psi_k\psi_k\,dt + \int_{t_k}^{t_{k+1}} \partial_t\psi_k\psi_k\,dt = \frac{1}{\tau}\int_{t_{k-1}}^{t_k} \frac{t-t_{k-1}}{t_k-t_{k-1}}\,dt - \frac{1}{\tau}\int_{t_{k-1}}^{t_k} \frac{t_{k+1}-t}{t_{k+1}-t_k}\,dt = 0.
\end{aligned}
\tag{37}
$$

By replacing in I_3 the integrals $\sum_{k,l=1}^{N}\int_{t_{k-1}}^{t_{k+1}}\partial_t\psi_k(t)\psi_l(t)\,dt$ with their explicit expression through (37) we get the term $(\mathbf{E}^{k+1}-\mathbf{E}^{k-1})/2$ in the last term of (36). In a similar way we obtain the term $\tau(\mathbf{E}^{k-1}/6+2\mathbf{E}^{k}/3+\mathbf{E}^{k+1}/6)$ in (36), which corresponds to the explicitly computed terms of the mass matrix in time $\sum_{k,l=1}^{N}\int_{t_{k-1}}^{t_{k+1}}\psi_k(t)\psi_l(t)\,dt$. Additional τ at the right hand side of (36) appears after the explicit computing of the time integrals $\sum_{k,l=1}^{N}\int_{t_{k-1}}^{t_{k+1}}\partial_t\psi_k(t)\partial_t\psi_l(t)\,dt$. This also gives terms $\mathbf{E}^{k+1}-2\mathbf{E}^{k}+\mathbf{E}^{k-1}$ at the left hand side of (36).

Let us define the mapping F_K such that $F_K(\widehat{K})=K$ and let $\widehat{\varphi}$ be the piecewise linear local basis function on the reference element $\widehat{K}$ such that $\varphi\circ F_K=\widehat{\varphi}$. Then, at the element level K, the matrix entries in (36) are explicitly given by:

$$
\begin{aligned}
M^K_{i,j} &= \left(\varepsilon_i\varphi_i\circ F_K,\ \varphi_j\circ F_K\right)_K, & M^{\partial\Omega}_{i,j} &= \left(\varphi_i\circ F_K,\ \varphi_j\circ F_K\right)_{\partial\Omega_K},\\
D^K_{i,j} &= \left(\nabla\cdot\varphi_i\circ F_K,\ \nabla\cdot\varphi_j\circ F_K\right)_K, & G^K_{i,j} &= \left(\nabla\varphi_i\circ F_K,\ \nabla\varphi_j\circ F_K\right)_K,\\
C^K_{i,j} &= \left(\nabla\cdot(\varepsilon_i\varphi_i)\circ F_K,\ \nabla\cdot\varphi_j\circ F_K\right)_K, & F^K_{j,m} &= (j,\varphi_j)_K.
\end{aligned}
$$

To obtain an explicit scheme we approximate M by the lumped mass matrix M^L in space, i.e., the diagonal approximation obtained by taking the row sum of M [13, 17]. We use the mass lumping as well in time by replacing terms corresponding to the mass matrix in time, $\mathbf{E}^{k-1}6+2\mathbf{E}^{k}/3+\mathbf{E}^{k+1}/6$, by $\mathbf{E}^{k}$.

Next, by multiplying (36) with $(M^L)^{-1}$, we obtain the following fully explicit time-stepping method to solve (11)–(14):

$$
\begin{aligned}
\mathbf{E}^{k+1}\left(1-\frac{1}{2}\tau M^{\partial\Omega}(M^L)^{-1}\right) &= -\tau^2(M^L)^{-1}F^k+2\mathbf{E}^k+\tau^2(M^L)^{-1}D\mathbf{E}^k-\tau^2(M^L)^{-1}G\mathbf{E}^k\\
&\quad -s\tau^2(M^L)^{-1}C\mathbf{E}^k-\left(1+\frac{1}{2}\tau M^{\partial\Omega}(M^L)^{-1}\right)\mathbf{E}^{k-1}.
\end{aligned}
\tag{38}
$$

In the case when (38) is used only in Ω_{FEM} in the hybrid FEM/FDM, it reduces to the following scheme:

$$
\mathbf{E}^{k+1}=-\tau^2(M^L)^{-1}F^k+2\mathbf{E}^k+\tau^2(M^L)^{-1}D\mathbf{E}^k-\tau^2(M^L)^{-1}G\mathbf{E}^k-s\tau^2(M^L)^{-1}C\mathbf{E}^k-\mathbf{E}^{k-1}. \tag{39}
$$

5.2. Finite difference formulation

We recall, see Section 3, that in Ω_{FDM} we have $\varepsilon(x)=\mu(x)=1$. Thus in Ω_{FDM} we have to solve a system of vector wave equations for the vector field $E=(E_1,E_2,E_3)$:

$$
\partial_t^2E-\Delta E=-j, \tag{40}
$$

$$
E(x,0)=0,\qquad E_t(x,0)=0,\qquad \text{in}\quad \Omega,
$$

$$
\partial_nE(x,t)=-\partial_tE(x,t),\qquad \text{on}\quad \partial\Omega_T. \tag{41}
$$

Using standard finite difference discretization of equation (40) in Ω_{FDM} we obtain the following explicit scheme:

$$
E^{k+1}_{i,j,m}=-\tau^2j^k_{i,j,m}+\tau^2\Delta E^k_{i,j,m}+2E^k_{i,j,m}-E^{k-1}_{i,j,m}, \tag{42}
$$

where $E^k_{i,j,m}$ is the solution on the time iteration k at the discrete point (i,j,m), $j^k_{i,j,m}$ is the discrete analog of the function j, τ is the time step, and $\Delta E^k_{i,j,m}$ is the discrete Laplacian. In three dimensions, to approximate $\Delta E^k_{i,j,m}$ we get the standard seven-point stencil

$$
\Delta E^k_{i,j,m}=\frac{E^k_{i+1,j,m}-2E^k_{i,j,m}+E^k_{i-1,j,m}}{dx^2}+\frac{E^k_{i,j+1,m}-2E^k_{i,j,m}+E^k_{i,j-1,m}}{dy^2}+\frac{E^k_{i,j,m+1}-2E^k_{i,j,m}+E^k_{i,j,m-1}}{dz^2},
$$

where dx, dy, and dz are the steps of discrete finite difference meshes in the directions x, y, z, respectively.

5.3. Absorbing boundary conditions

To discretize absorbing boundary condition (41) in Ω_{FDM} we use a forward finite difference approximation at the middle point, which gives a numerical approximation of higher order than an ordinary (backward or forward) finite difference approximation. For example, for the left boundary of Ω_{FDM} we have the following variant of condition (41):

$$\frac{\partial E(x,t)}{\partial x} = \frac{\partial E(x,t)}{\partial t}.$$

Then we use the following finite difference discretization of the above equation:

$$\frac{E^{k+1}_{i,j,m} - E^{k}_{i,j,m}}{dt} + \frac{E^{k+1}_{i+1,j,m} - E^{k}_{i+1,j,m}}{dt} - \frac{E^{k}_{i+1,j,m} - E^{k}_{i,j,m}}{dx} - \frac{E^{k+1}_{i+1,j,m} - E^{k+1}_{i,j,m}}{dx} = 0,$$

which can be transformed to

$$E^{k+1}_{i,j,m} = E^{k}_{i+1,j,m} + E^{k}_{i,j,m}\frac{dx-dt}{dx+dt} - E^{k+1}_{i+1,j,m}\frac{dx-dt}{dx+dt}.$$

For other boundaries of Ω_{FDM}, boundary condition (41) can be written similarly.

6. The domain decomposition FEM/FDM

We now describe the data communication for the solution to problem (11)–(14) between the finite element method on the unstructured part of the mesh, Ω_{FEM}, and the finite difference method on the structured part, Ω_{FDM}. This communication is achieved by mesh overlapping across a two-element thick layer around Ω_{FEM}, see Figure 1.

First, using Figure 1, we observe that the interior nodes of the computational domain Ω belong to either of the following sets:

- ω_o nodes 'o' interior to Ω_{FDM} that lie on the boundary of Ω_{FEM},
- $\omega_\times$ nodes '$\times$' interior to Ω_{FEM} that lie on the boundary of Ω_{FDM},
- ω_* nodes '$*$' interior to Ω_{FEM} that are not contained in Ω_{FDM},
- ω_D nodes 'D' interior to Ω_{FDM} that are not contained in Ω_{FEM}.

We also note that because we are using the explicit domain decomposition FEM/FDM we need to choose the time step τ such that the whole scheme remains stable. We use the stability analysis on the structured meshes and choose the largest time step in our computations accordingly to the CFL stability condition [2]

$$\tau \le \frac{\sqrt{\varepsilon\mu}}{\sqrt{1/dx^2 + 1/dy^2 + 1/dz^2}}. \tag{43}$$

Usually, we have $dx = dy = dz = h$, and condition (43) can be rewritten in three dimensions as

$$\tau \le h\sqrt{\frac{\varepsilon\mu}{3}}. \tag{44}$$

Algorithm

At every time step we perform the following operations:

(a) On the structured part of the mesh Ω_{FDM}, compute E^{k+1} from (42) with absorbing boundary condition (41) at $\partial\Omega$, with E^k and E^{k-1} known.

(b) On the unstructured part of the mesh Ω_{FEM}, compute E^{k+1} by using the explicit finite element scheme (39) with E^k and E^{k-1} known.

(c) Use the values of the electric field E^{k+1} at nodes $\omega_\times$, which are computed using the finite element scheme (39), as a boundary condition for the finite difference method in Ω_{FDM}.

(d) Use the values of the electric field E^{k+1} at nodes ω_o, which are computed using the finite difference scheme (42), as a boundary condition for the finite element method in Ω_{FEM}.

(e) Apply swap of the solutions for the electric field in order to apply the algorithm on a new time level k.

7. Numerical studies

In all our two-dimensional tests we choose the computational domain $\Omega = [-8.0, 8.0] \times [-8.0, 8.0]$. This domain is split into a finite element subdomain $\Omega_{FEM} = [-3.5, 3.5] \times [-3.5, 3.5]$ and a surrounding region Ω_{FDM} with a structured mesh, $\Omega = \Omega_{FEM} \cup \Omega_{FDM}$, see Figure 2.

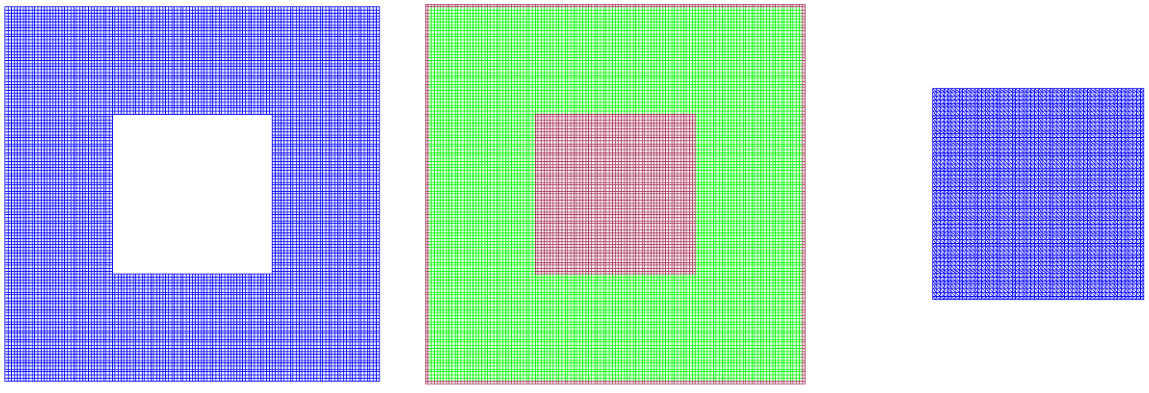

a) Ω_{FDM} b) $\Omega = \Omega_{FEM} \cup \Omega_{FDM}$ c) Ω_{FEM}

Figure 2. The hybrid mesh b) is a combination of a structured mesh a), where FDM is applied, and a mesh c), where we use FEM, with two layers of overlapping structured elements. The coefficient $\varepsilon(x)$ in (31) is given as follows: $\varepsilon(x) = 1$ in Ω_{FDM} and $\varepsilon(x) \geq 1$ for $x \in \Omega \setminus \Omega_{FDM}$.

The spatial mesh in Ω consists of triangles and in Ω_{FDM} of squares. The boundary of the domain Ω is $\partial\Omega = \partial\Omega_1 \cup \partial\Omega_2 \cup \partial\Omega_3$. Here, $\partial\Omega_1$ and $\partial\Omega_2$ are the top and the bottom sides of Ω, and $\partial\Omega_3$ is the union of the left and right sides of this domain, see Figure 2. Let us define $\Omega_{FEM_T} = \Omega_{FEM} \times (0, T)$ and $\Omega_{FDM_T} = \Omega_{FDM} \times (0, T)$.

We also denote different boundaries in the domain decomposition method, see Section 6 for details, as follows: the boundary of Ω_{FEM} by $\partial\Omega_{FEM}$, the outer boundary of Ω_{FDM} by $\partial\Omega$, the inner boundary of Ω_{FDM} by $\partial\Omega_{FDM}$, nodes corresponding to $\partial\Omega_{FEM}$ but which lie in Ω_{FDM} by $\partial\Omega_{\omega_0}$, and the nodes corresponding to $\partial\Omega_{FDM}$ but which lie in Ω_{FEM} by $\partial\Omega_{\omega_x}$. Next, let $\partial\Omega_{FDM_T} = \partial\Omega_{FDM} \times (0, T)$, $\partial\Omega_{FEM_T} = \partial\Omega_{FEM} \times (0, T)$, $\partial\Omega_{\omega_x T} = \partial\Omega_{\omega_x} \times (0, T)$, and $\partial\Omega_{\omega_0 T} = \partial\Omega_{\omega_0} \times (0, T)$. In all our computational tests we choose the penalty factor $s = 1$.

7.1. Numerical studies with exact smooth solution

In computational tests of this section we solve Maxwell's system (6) in Ω during time $T = [0, 20]$ in two dimensions with the known smooth solution

$$E_1(x, y, t) = \frac{t^2}{2.0} \cos(\pi x) \cdot \sin(\pi y), \qquad E_2(x, y, t) = -\frac{t^2}{2.0} \sin(\pi x) \cdot \cos(\pi y).$$

In this case, problem (6) for the electric field in Ω_{FEM} reduces to the following problem in two dimensions:

$$\begin{aligned}
\varepsilon \frac{\partial^2 E_1}{\partial t^2} + \frac{\partial}{\partial y}\left(\frac{\partial E_2}{\partial x} - \frac{\partial E_1}{\partial y}\right) &= (\varepsilon + t^2\pi^2) \cdot \cos(\pi x) \cdot \sin(\pi y), && \text{in} \quad \Omega_{\text{FEM}_T}, \\
\varepsilon \frac{\partial^2 E_2}{\partial t^2} - \frac{\partial}{\partial x}\left(\frac{\partial E_2}{\partial x} - \frac{\partial E_1}{\partial y}\right) &= -(\varepsilon + t^2\pi^2) \cdot \sin(\pi x) \cdot \cos(\pi y), && \text{in} \quad \Omega_{\text{FEM}_T}, \\
E(x, 0) = 0, \qquad E_t(x, 0) &= 0, && \text{in} \quad \Omega_{\text{FEM}}, \\
\nabla \cdot (\epsilon E) &= 0, && \text{in} \quad \Omega_{\text{FEM}_T}, \\
E(x, t)\restriction_{\partial\Omega_{\text{FEM}_T}} &= E(x, t)\restriction_{\partial\Omega_{\omega_{0T}}}.
\end{aligned} \tag{45}$$

In Ω_{FDM} our coefficients are $\varepsilon = \mu = 1$, and in this domain we have to solve the following problem:

$$\begin{aligned}
\partial_{tt} E_1 - \Delta E_1 &= (\varepsilon + t^2\pi^2) \cdot \cos(\pi x) \cdot \sin(\pi y), && \text{in} \quad \Omega_{\text{FDM}_T}, \\
\partial_{tt} E_2 - \Delta E_2 &= -(\varepsilon + t^2\pi^2) \cdot \sin(\pi x) \cdot \cos(\pi y), && \text{in} \quad \Omega_{\text{FDM}_T}, \\
E(x, 0) = 0, \qquad E_t(x, 0) &= 0, && \text{in} \quad \Omega_{\text{FDM}}, \\
E(x, t)\restriction_{\partial\Omega_{\text{FDM}_T}} &= E(x, t)\restriction_{\partial\Omega_{\omega_{xT}}}, \\
\partial_n E &= -\partial_t u, && \text{on} \quad \partial\Omega_T.
\end{aligned}$$

From system (45) we see that in Ω_{FEM} the solution E is initialized by the non-zero solution for the electric field obtained by the finite difference method in Ω_{FDM} and thus the initialized finite element solution is also nonzero. To solve (45), we modify these equations and add the penalty term $s\nabla(\nabla \cdot (\epsilon E))$, similarly as with equation (7). We choose the time step $\tau = 0.02$ corresponding to the CFL condition (44), while the penalty factor is always set to $s = 1$.

7.1.1. Test 1

In this test we use the domain decomposition method with the coefficient $\varepsilon(x)$ defined as a function inside Ω_{FEM} such that

$$\varepsilon(x) = \begin{cases} 1 + A \sin^2 \dfrac{\pi x}{3} \cdot \sin^2 \dfrac{\pi y}{3}, & 0 \le x \le 3, \quad -3 \le y \le 0, \\ 1, & \text{at all other points}, \end{cases} \tag{46}$$

with amplitude values $A = 3, 12, 26, 37, 51$, see Figure 3 a) for this function in the case when amplitude $A = 3$ in (46).

First we perform computations on the mesh with mesh size $h = 0.125$. Figures 4 demonstrate the continuity of the computed components of the vector field (E_1, E_2) across the Finite Difference/Finite Element mesh in the domain decomposition method with $A = 3$ in (46) at different times. We observe that the components of the vector field (E_1, E_2) remain smooth across the FE/FD interface at all times. We also observe that the exact components of the vector field look very similar to the computed ones, compare Figures 4.

Figures 5 show the vector field (E_1, E_2) of the computed solution in the domain decomposition method compared with the exact ones at different times. We observe the smoothness of the vector field when computing with $A = 3$ in (46). Figure 10 shows the time evolution of the intensity of the exact electric field $|E| = \sqrt{E_1^2 + E_2^2}$ compared with the simulated solution

$$|E_h| = \sqrt{E_{h1}^2 + E_{h2}^2}. \tag{47}$$

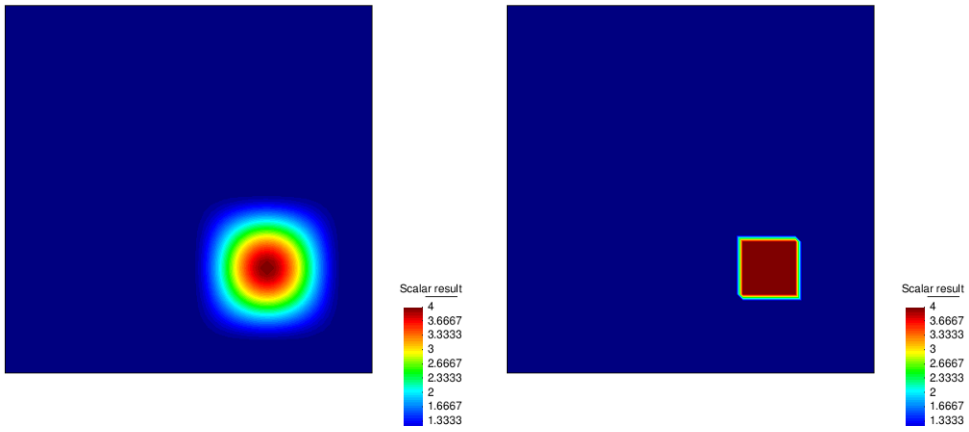

a) $\max \varepsilon = 4$ in Test 1 b) $\varepsilon = 4$ in Test 2

Figure 3. Coefficient $\varepsilon(x)$ in different tests.

The solution is presented at different points of the computational domain Ω_{FEM}. Figure 11 a) shows corresponding to Figure 10 computed relative L_2-norms in Ω_{FEM} during time $T = (0, 20)$. Relative L_2-norms are defined as $\|E - E_h\|_{L_2(\Omega_{FEM})}/\|E\|_{L_2(\Omega_{FEM})}$, where E and E_h are the exact and computed intensities of the electric fields, correspondingly. Figure 11 b) shows the computed L_2-norms of $E - E_h$ in Ω_{FEM} during time $T = (0, 20)$. From Figures 4–8, 11 we can conclude that the computed solution E_h is very close to the exact one E as long as values of the coefficient ε are not too big ($A < 26$ in (46)), and the final time T is also not very large ($T < 10$).

Let us compare Figure 9 with Figure 8. In Figure 8 we observe the appearance of the spurious modes when computing the domain decomposition method on the mesh with the mesh size $h = 0.125$, with large times ($T > 8$) and with large amplitude values ($A > 12$) in (46). However, these spurious solutions are removed as the mesh is refined, see Figure 9.

7.1.2. Test 2

In this test we use the domain decomposition method when $\varepsilon = 1$ in Ω except for one small square in Ω_{FEM}, where $\varepsilon = A$ with $A = 3, 12, 26, 37, 51$, see Figure 3 b) for example of this coefficient in the case when $\varepsilon = 4$ inside the small square. In other words, the coefficient ε is defined inside Ω_{FEM} as

$$\varepsilon(x) = \begin{cases} 1 + A, & 0 \le x \le 3, \quad -3 \le y \le 0, \\ 1, & \text{at all other points,} \end{cases}$$

with amplitude values $A = 3, 12, 26, 37, 51$.

In this case we have similar behavior of the electric field as in Test 1 even in case of discontinuous coefficient ε in the model equations. In all cases of this test we have continuity of the computed solution across FEM/FDM mesh, and its behavior is very similar to the behavior of the solution presented in all figures related to Test 1. Thus, we do not present these solutions again. From this test we can conclude that the computed solution E_h on the mesh with mesh size $h = 0.125$ is very close to the exact solution E as long as discontinuity in the coefficient ε is not big ($\varepsilon < 26$) and the computational time T is not very large ($T < 10$). However, when the mesh is refined these spurious solutions disappear, even when computing the model problem with large values of the amplitude A in a small square in Ω_{FEM}.

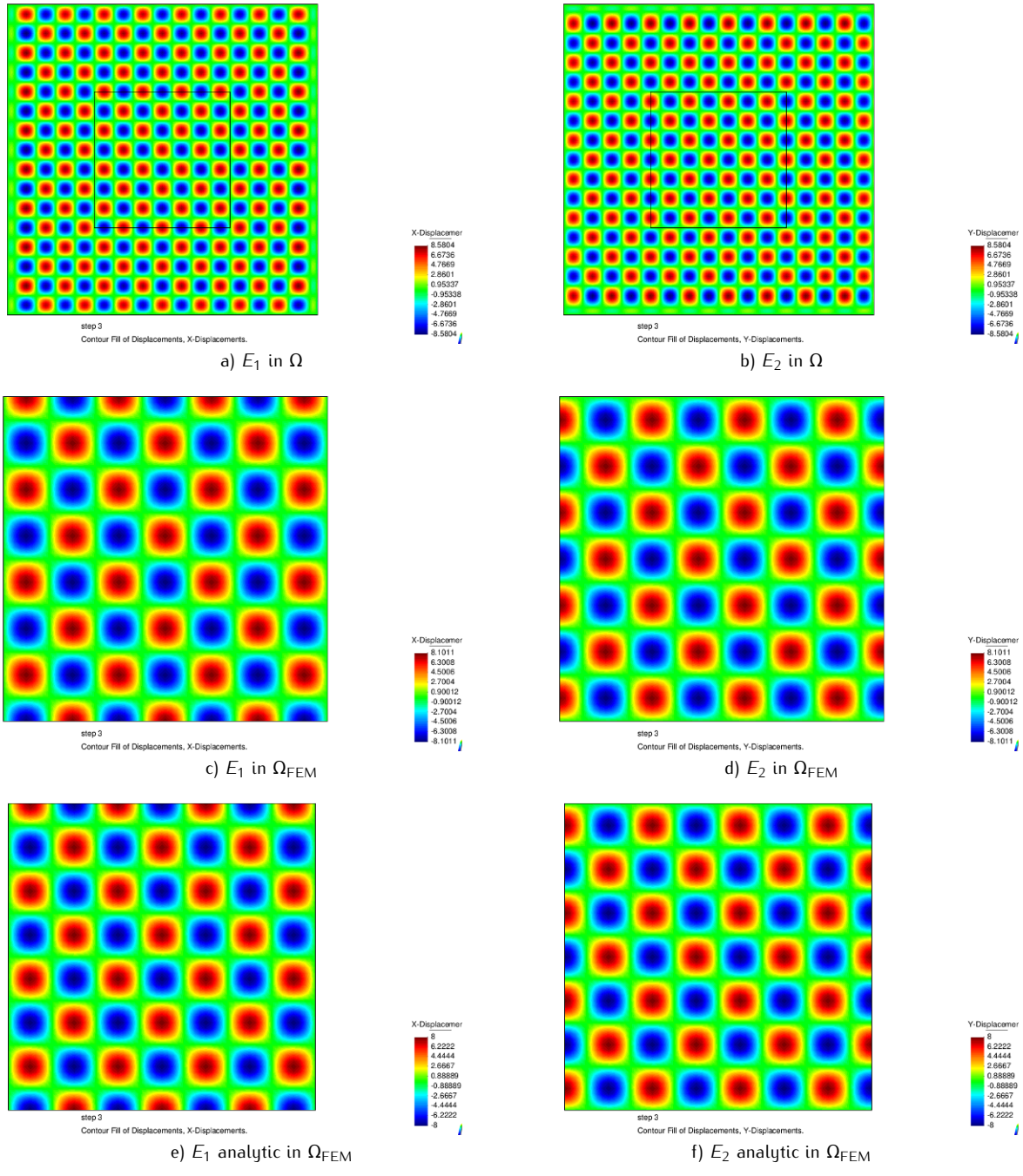

Figure 4. **Test 1.** Comparison of the analytic solution (E_1, E_2) versus the computed solution (E_{1h}, E_{2h}) in the domain decomposition FEM/FDM at time moment $t = 8.0$ for $A = 3$ in (46). We present: in a) and b) components (E_{1h}, E_{2h}) in Ω; in c) and d) components (E_{1h}, E_{2h}) of the finite element solution in Ω_{FEM}, and in e) and f) components (E_1, E_2) of the analytic solution in Ω_{FEM}.

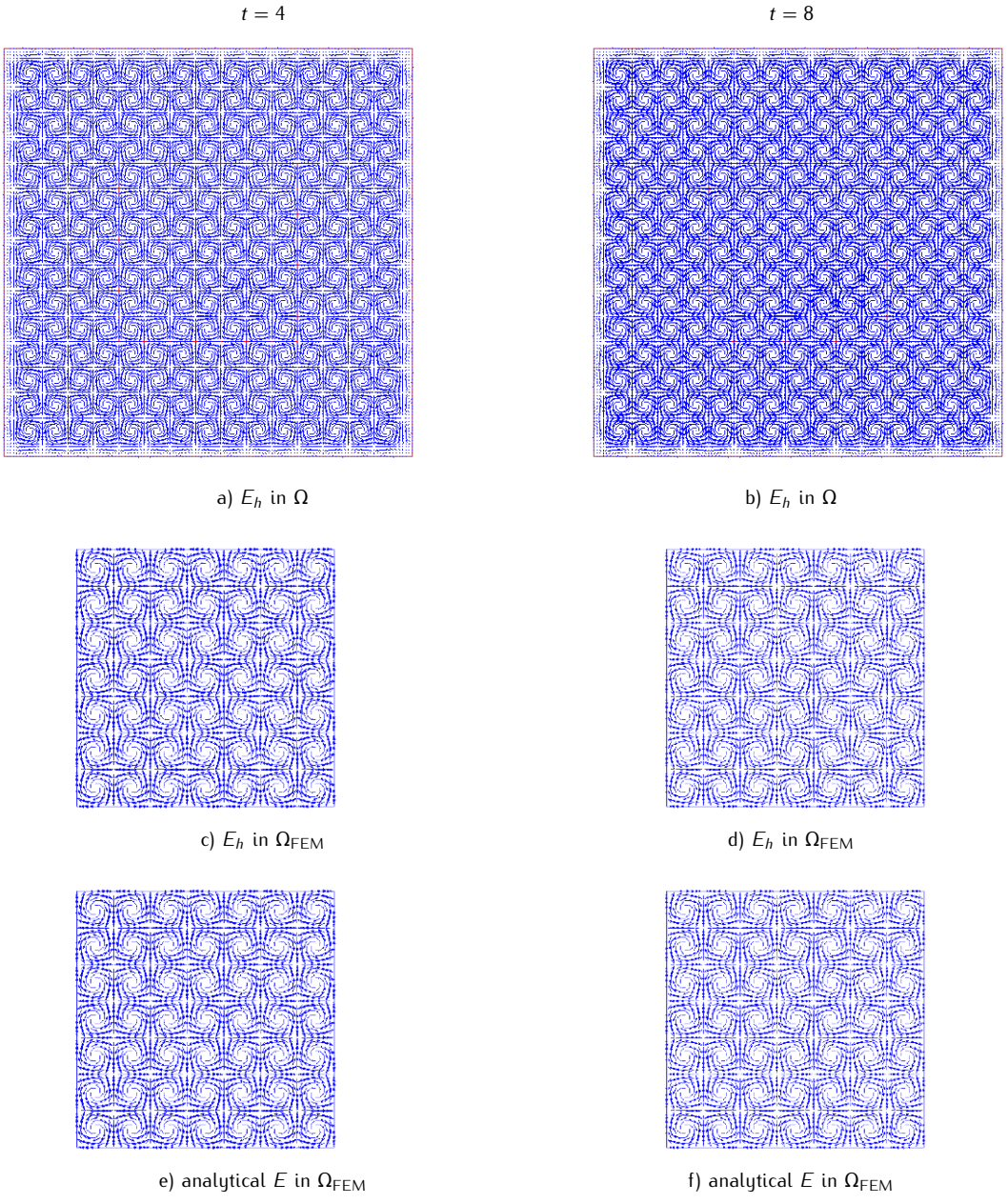

Figure 5. **Test 1.** Behavior of the computed vector electric field $E_h = (E_{1h}, E_{2h})$ and the analytical one in the domain decomposition FEM/FDM at time moments $t = 4.0$ and $t = 8$, respectively. We show in a) and b) the computed vector electric field $E_h = (E_{1h}, E_{2h})$ in the domain decomposition FEM/FDM in Ω. In c) and d) the computed vector electric field $E_h = (E_{1h}, E_{2h})$ is shown in Ω_{FEM}. In e) and f) the analytical vector field $E = (E_1, E_2)$ is presented in Ω_{FEM}.

7.2. Numerical studies with a plane wave

In the tests of this section we solve problem (31)–(33) in Ω during time $T = [0, 20]$ in two dimensions with the plane wave $f(t)$ defined as

$$f(t) = \begin{cases} \sin(\omega t), & \text{if} \quad t \in (0, 2\pi/\omega), \\ 0, & \text{if} \quad t > 2\pi/\omega. \end{cases} \tag{48}$$

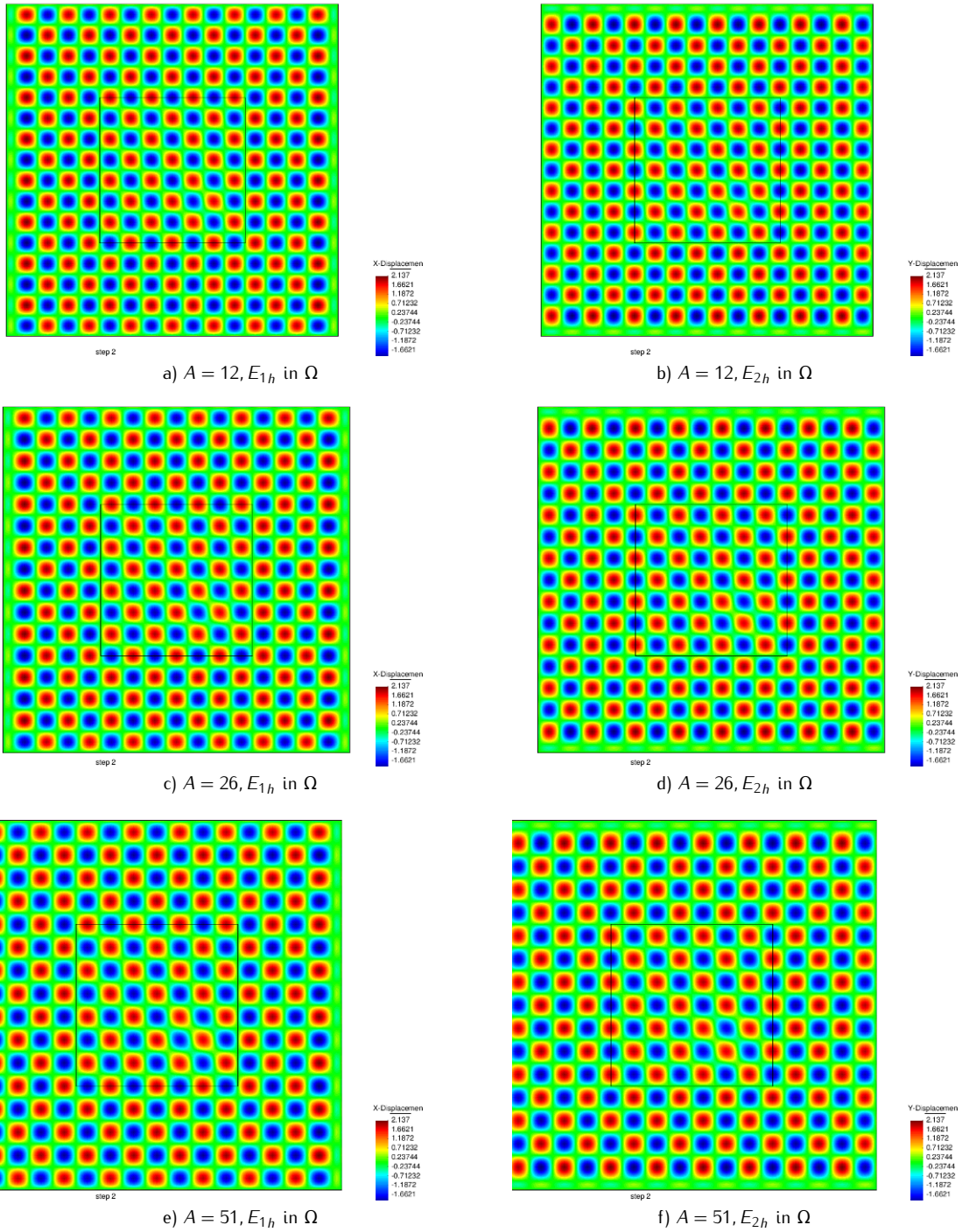

a) $A = 12, E_{1h}$ in Ω

b) $A = 12, E_{2h}$ in Ω

c) $A = 26, E_{1h}$ in Ω

d) $A = 26, E_{2h}$ in Ω

e) $A = 51, E_{1h}$ in Ω

f) $A = 51, E_{2h}$ in Ω

Figure 6. **Test 1.** Computed solutions $E_h = (E_{1h}, E_{2h})$ in the domain decomposition FEM/FDM at time moment $t = 4.0$ in Ω. We show comparisons of the computed solutions versus different values of the coefficient $\varepsilon(x)$ inside Ω_{FEM} for Maxwell's equations: in a) and b) the amplitude $A = 26$ in (46); in c) and d) the amplitude $A = 51$ in (46).

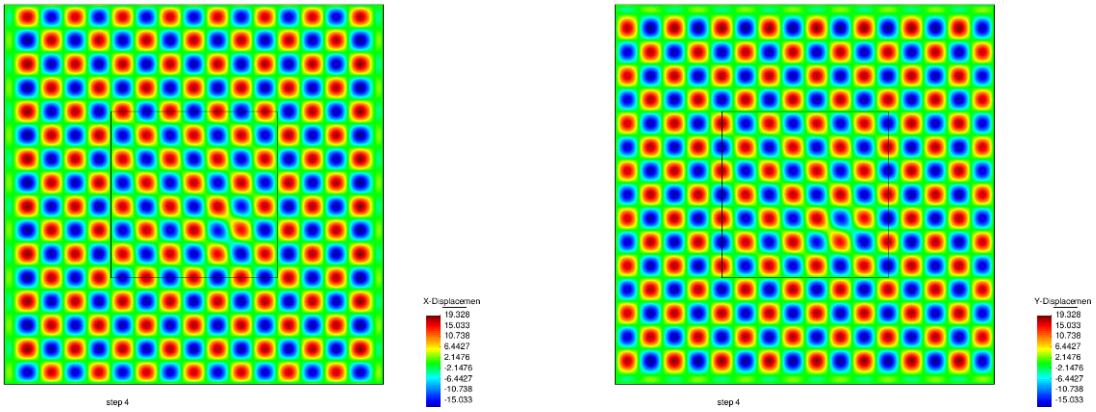

a) $A = 12, E_{1h}$ in Ω b) $A = 12, E_{2h}$ in Ω

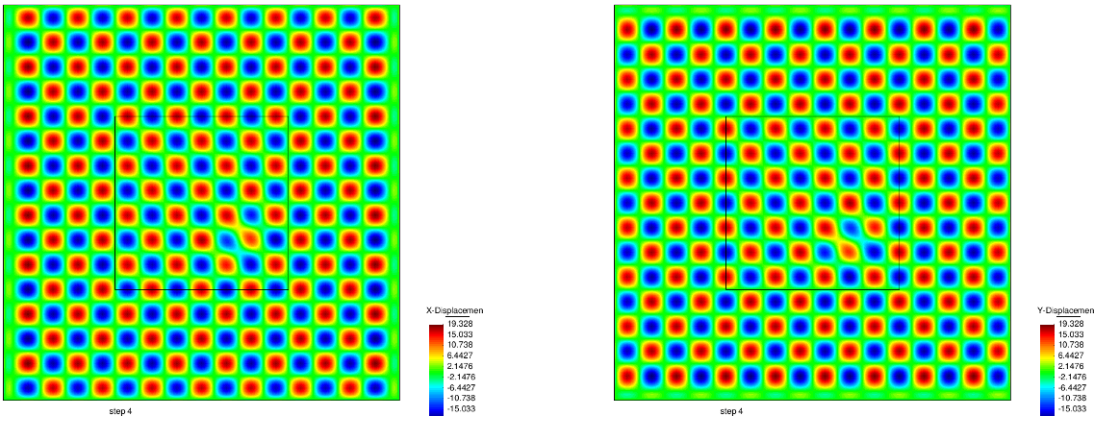

c) $A = 26, E_{1h}$ in Ω d) $A = 26, E_{2h}$ in Ω

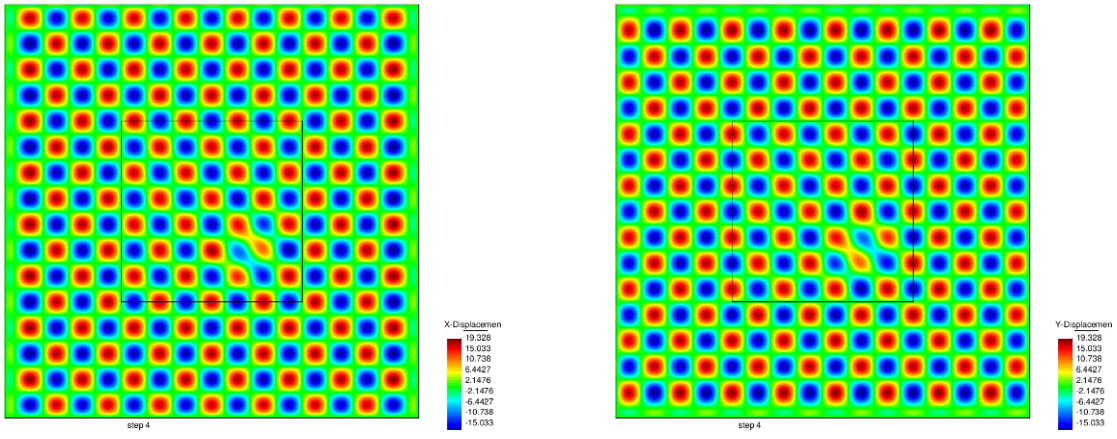

e) $A = 51, E_{1h}$ in Ω f) $A = 51, E_{2h}$ in Ω

Figure 7. **Test 1.** Computed solutions $E_h = (E_{1h}, E_{2h})$ in the domain decomposition FEM/FDM at time moment $t = 8.0$ in Ω. We show comparisons of the computed solutions versus different values of the coefficient $\varepsilon(x)$ inside Ω for Maxwell's equations: in a) and b) the amplitude $A = 26$ in (46); in c) and d) $A = 51$ in (46).

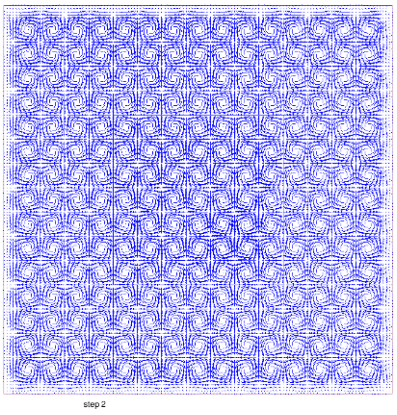

a) $A = 26, T = 4$

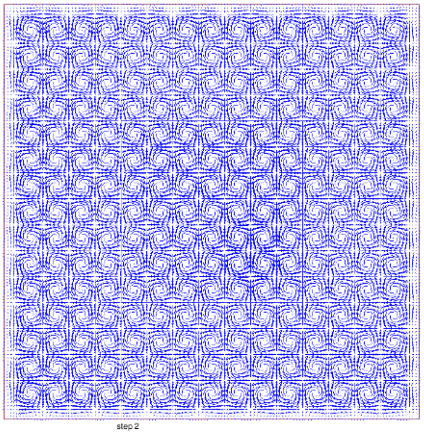

b) $A = 51, T = 4$

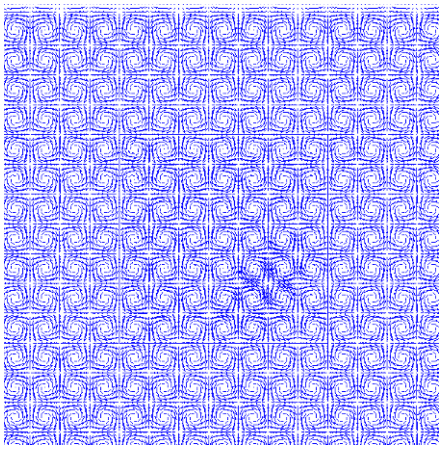

c) $A = 26, T = 8$

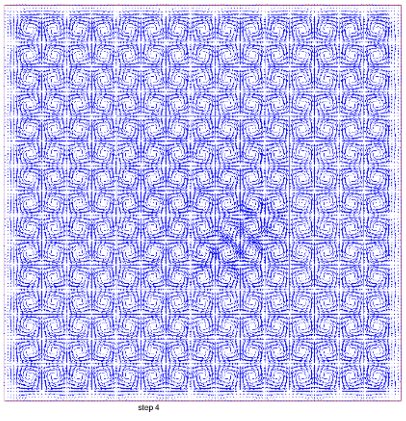

d) $A = 51, T = 8$

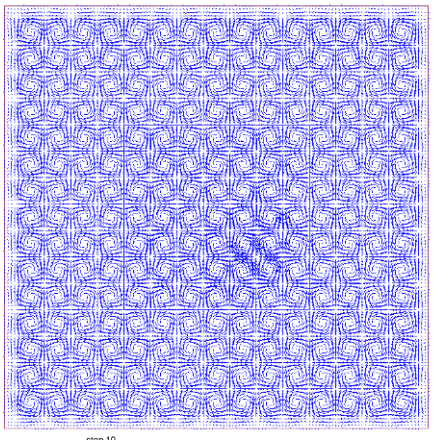

e) $A = 26, T = 20$

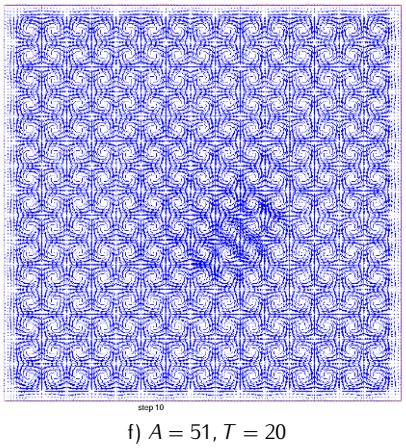

f) $A = 51, T = 20$

Figure 8. **Test 1.** Behavior of the computed vector electric field $E_h = (E_{1h}, E_{2h})$ in the domain decomposition FEM/FDM in Ω at different time moments. We show the electric vector field for different amplitude values A in (46) in Ω.

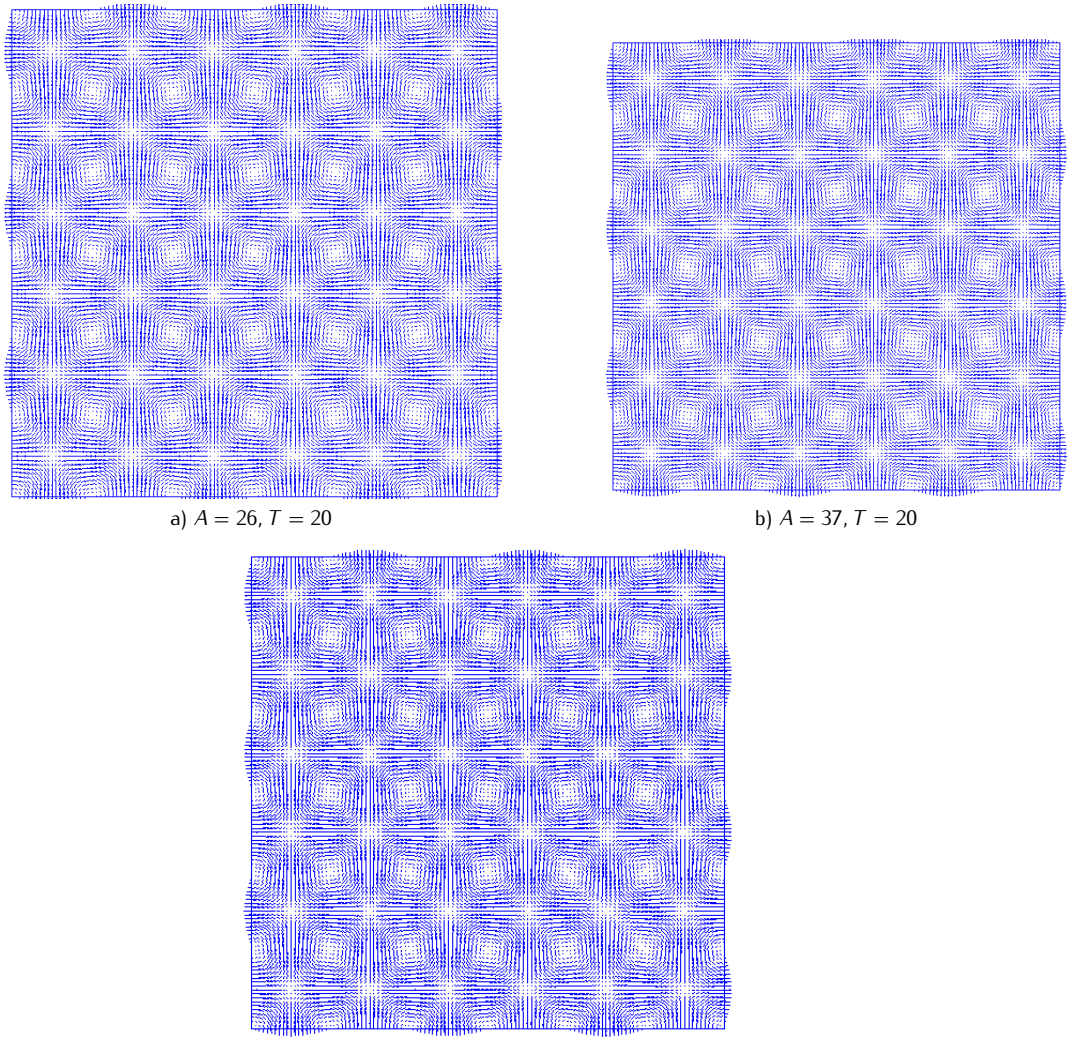

a) $A = 26$, $T = 20$ b) $A = 37$, $T = 20$

c) $A = 51$, $T = 20$

Figure 9. **Test 1.** Removal of spurious solutions on the finer mesh with the mesh size $h = 0.05$. We show the behavior of the computed vector electric field $E_h = (E_{1h}, E_{2h})$ in the domain decomposition FEM/FDM in Ω_{FEM} at $T = 20$. The electric vector field for different values of the amplitude A in (46) is presented in Ω. Compare with Figure 8, where spurious modes appeared already at time $T = 8$ (there computations were performed on the coarser mesh with mesh size $h = 0.125$).

In Ω_{FDM} our coefficients are $\varepsilon = \mu = 1$, and in this domain we have to solve the following problem:

$$
\begin{aligned}
E_{tt} - \Delta E &= 0, && \text{in} \quad G \times (0, T),\\
E(x,0) = 0, \quad E_t(x,0) &= 0, && \text{in} \quad G,\\
E_1 = 0, \quad E_2(x,t) &= f(t), && \text{on} \quad \partial\Omega_1 \times (0, t_1],\\
\partial_n E(x,t) &= -\partial_t u(x,t), && \text{on} \quad \partial\Omega_1 \times (t_1, T),\\
\partial_n E(x,t) &= -\partial_t u(x,t), && \text{on} \quad \partial\Omega_2 \times (0, T),\\
\partial_n u(x,t) &= 0, && \text{on} \quad \partial\Omega_3 \times (0, T),
\end{aligned}
\tag{49}
$$

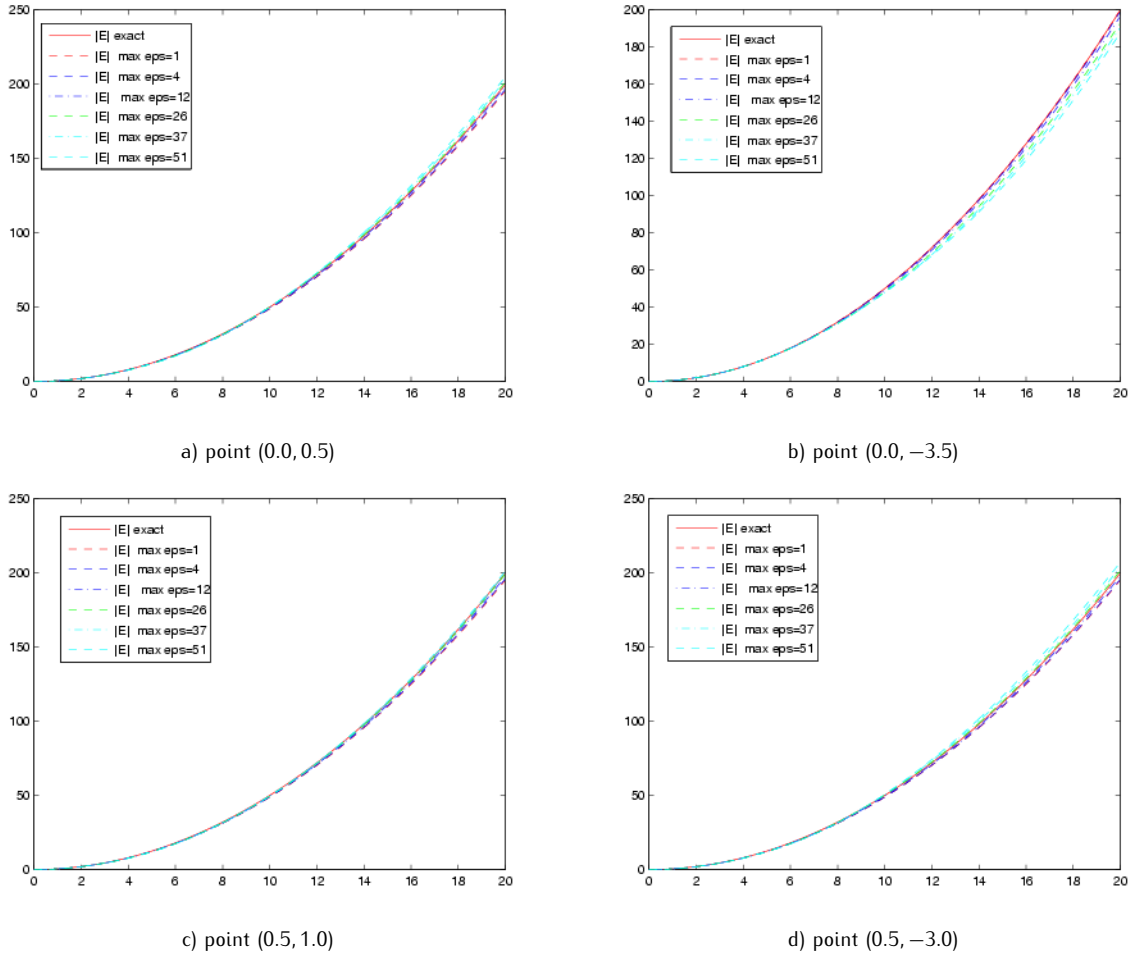

a) point $(0.0, 0.5)$ b) point $(0.0, -3.5)$

c) point $(0.5, 1.0)$ d) point $(0.5, -3.0)$

Figure 10. Test 1. Behavior of the exact and computed (47) solutions to equation (45) during $T = (0, 20)$: a) at the point $(0.0, 0.5)$, which is located at the center of the computational domain Ω_{FEM}; b) at the point $(0.0, -3.5)$, which is located at the bottom boundary of Ω_{FEM}; c) at the point $(0.5, 1.0)$, which is located close to the center of Ω_{FEM}; d) at the point $(0.5, -3.0)$, which is located at the lower part of Ω_{FEM}. We show the comparison of solutions with amplitude values $A = 4, 12, 26, 37, 51$ in (46). Here, the horizontal axis denotes the computation time.

and in Ω_{FEM} we have to solve

$$\begin{aligned}
\varepsilon \frac{\partial^2 E_1}{\partial t^2} + \frac{\partial}{\partial y}\left(\frac{\partial E_2}{\partial x} - \frac{\partial E_1}{\partial y}\right) - s\frac{\partial}{\partial x}\left(\frac{\partial(\epsilon E_1)}{\partial x} + \frac{\partial(\epsilon E_2)}{\partial y}\right) &= 0, \qquad \text{in} \quad \Omega_{\text{FEM}_T}, \\
\varepsilon \frac{\partial^2 E_2}{\partial t^2} - \frac{\partial}{\partial x}\left(\frac{\partial E_2}{\partial x} - \frac{\partial E_1}{\partial y}\right) - s\frac{\partial}{\partial y}\left(\frac{\partial(\epsilon E_1)}{\partial x} + \frac{\partial(\epsilon E_2)}{\partial y}\right) &= 0, \qquad \text{in} \quad \Omega_{\text{FEM}_T}, \\
E(x,0) = 0, \qquad E_t(x,0) = 0, \qquad &\text{in} \quad \Omega_{\text{FEM}}, \\
E(x,t)\restriction_{\partial\Omega_{\text{FEM}_T}} = E(x,t)\restriction_{\partial\Omega_{\omega_0 T}}&.
\end{aligned} \tag{50}$$

We choose the time step $\tau = 0.02$ in all tests corresponding to the CFL condition (44). The penalty factor s is always chosen to be 1. In the initialized plane wave (48) we take $\omega = 7$ in all tests.

First, in Test 3 we demonstrate that our computed solution E_h in the domain decomposition method approximates very well the exact solution E in the case when $\varepsilon = \mu = 1$ in Ω. Next, in Test 4 we demonstrate the validity of our method by simulating problem (49)–(50) in the presence of the function $\varepsilon(x) \neq 0$ in Ω_{FEM}.

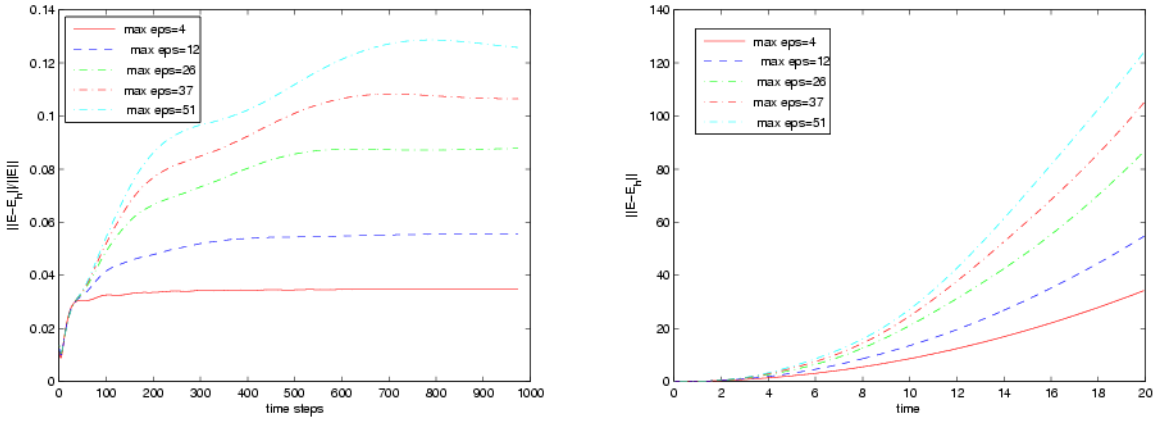

a) b)

Figure 11. Test 1. a) relative errors $\|E-E_h\|_{L_2(\Omega_{FEM})}/\|E\|_{L_2(\Omega_{FEM})}$ during time $T=(0,20)$; b) norms $\|E-E_h\|_{L_2(\Omega_{FEM})}$ during time $T=(0,20)$.

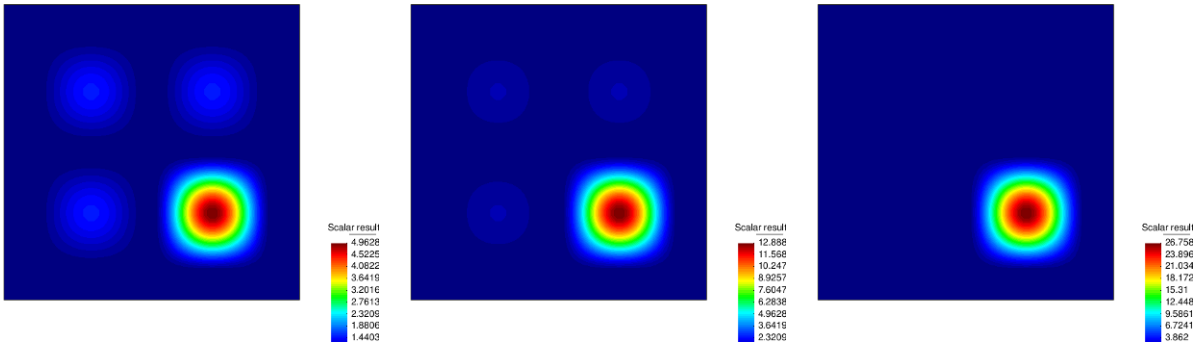

a) $A=4$ b) $A=12$ c) $A=26$

Figure 12. Different coefficients $\varepsilon(x)$ defined by (53) used in tests with a plane wave.

7.2.1. Test 3

In this test we compare our computational solution obtained in the domain decomposition method with the analytical solution. We compute problem (49)–(50) on two different meshes with different mesh sizes h, with $h=0.125$ and with $h=0.05$. The plane wave is defined as in (48).

The analytical solution to problem (49)–(50) with $\varepsilon=\mu=1$ reduces to the solution of the homogeneous wave equation and is given by the following formula, see [8]:

$$E_2(y,t)=\begin{cases}0, & \text{if} \quad t\in(0,a-y).\\ \sin\omega(t-a+y), & \text{if} \quad t\in(a-y,\,a-y+2\pi/\omega),\\ 0, & \text{if} \quad t>a-y+2\pi/\omega.\end{cases} \tag{51}$$

Here y is the vertical coordinate and we consider (49)–(50) on the domain $R_a=\{y<a\}$, $a=\text{const}\geq 0$, while $E_1=0$.

Figure 14 presents a comparison between the exact solution given by (51) and the computed solutions for (49)–(50), at different points of the computational domain Ω. We show the computed domain decomposition solution on different meshes with mesh sizes $h=0.125$ and $h=0.05$. We observe that the exact and computed solutions differ mainly at

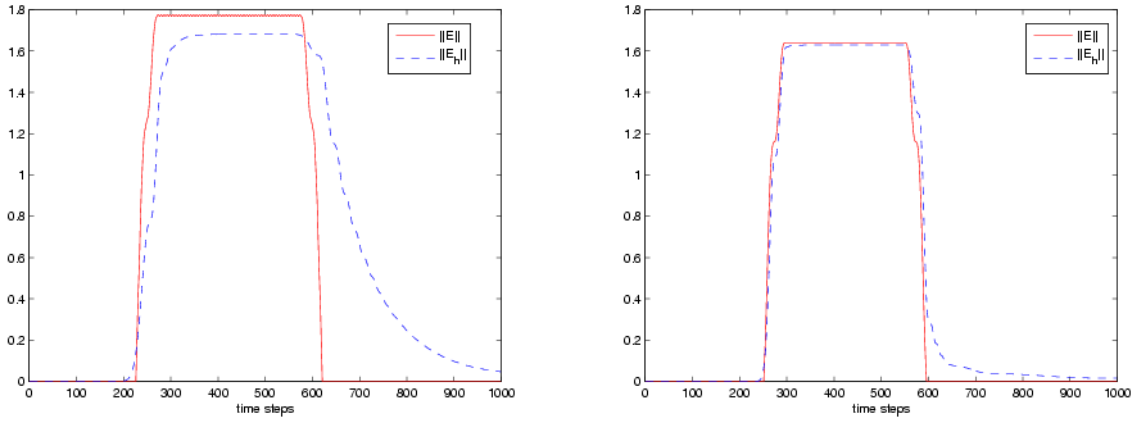

a) $h = 0.125$ b) $h = 0.05$

Figure 13. Test 3. Numerical comparisons of the computed L_2-norms for $\|E\|$ and $\|E_h\|$ on different meshes with mesh sizes $h = 0.125$ and $h = 0.05$, respectively. We show computed L_2-norms during time $T = (0, 20)$ in Ω_{FEM}. Here, the horizontal axis denotes the number of time steps in $T = (0, 20)$.

the bottom of the computational domain Ω_{FEM}. This can be explained by the fact that the computational error grows with computational time. Comparing a) & b) with c) & d) in Figure 14 we observe that the computed solution E_h on the mesh with mesh size $h = 0.125$ has amplitude approximately twice smaller than the exact solution E, but the computed solution on the mesh size $h = 0.05$ approximates more accurately the exact solution. The same observation is confirmed by Figure 13 a), which shows the comparison of the exact norm $\|E\|_{\Omega_{\text{FEM}}}$ and the computed norm $\|E_h\|_{\Omega_{\text{FEM}}}$ on different meshes with mesh sizes $h = 0.125$ and $h = 0.05$ during time $T = (0, 20)$.

This test shows that the FEM scheme used in the domain decomposition method is second order convergent in space and time, and the underlaying a posteriori error analysis for (50) is similar to the one developed in [2].

7.2.2. Test 4

The goal of this test is to explain why in some real-life experiments with the electromagnetic plane wave that propagates in the medium with the coefficient $\varepsilon \neq 0$ it is still possible to approximate Maxwell's system with the wave equation

$$\begin{aligned}
\varepsilon \frac{\partial^2 E}{\partial t^2} - \Delta E = 0, \quad & \text{in } \Omega_T, \\
E(x,0) = f_0(x), \quad E_t(x,0) = 0, \quad & \text{in } \Omega, \\
E(x,t) = f(t), \quad & \text{on } \partial\Omega_1 \times (0, t_1], \\
\partial_n E(x,t) = -\partial_t u(x,t), \quad & \text{on } \partial\Omega_1 \times (t_1, T), \\
\partial_n E(x,t) = -\partial_t u(x,t), \quad & \text{on } \partial\Omega_2 \times (0, T), \\
\partial_n u(x,t) = 0, \quad & \text{on } \partial\Omega_3 \times (0, T).
\end{aligned} \tag{52}$$

Such a model is considered in our recent publications [5, 18], where the spatially distributed dielectric constant was reconstructed from experimental data via a hybrid globally convergent/adaptive algorithm. In [5, 18] there were some discrepancies between the computational model and real-like experiments: instead of considering the globally convergent method for Maxwell's system (6), in [5, 18] we used the model of the single wave equation (52). Moreover, it was not known which one of the three components of the electric field was measured in experiments. The fact that in [5, 18] a very accurate reconstruction of the dielectric constant still was obtained demonstrates validity of the approximated model. Our tests below in 2D and 3D demonstrate an explanation of the experiment performed in [5, 18].

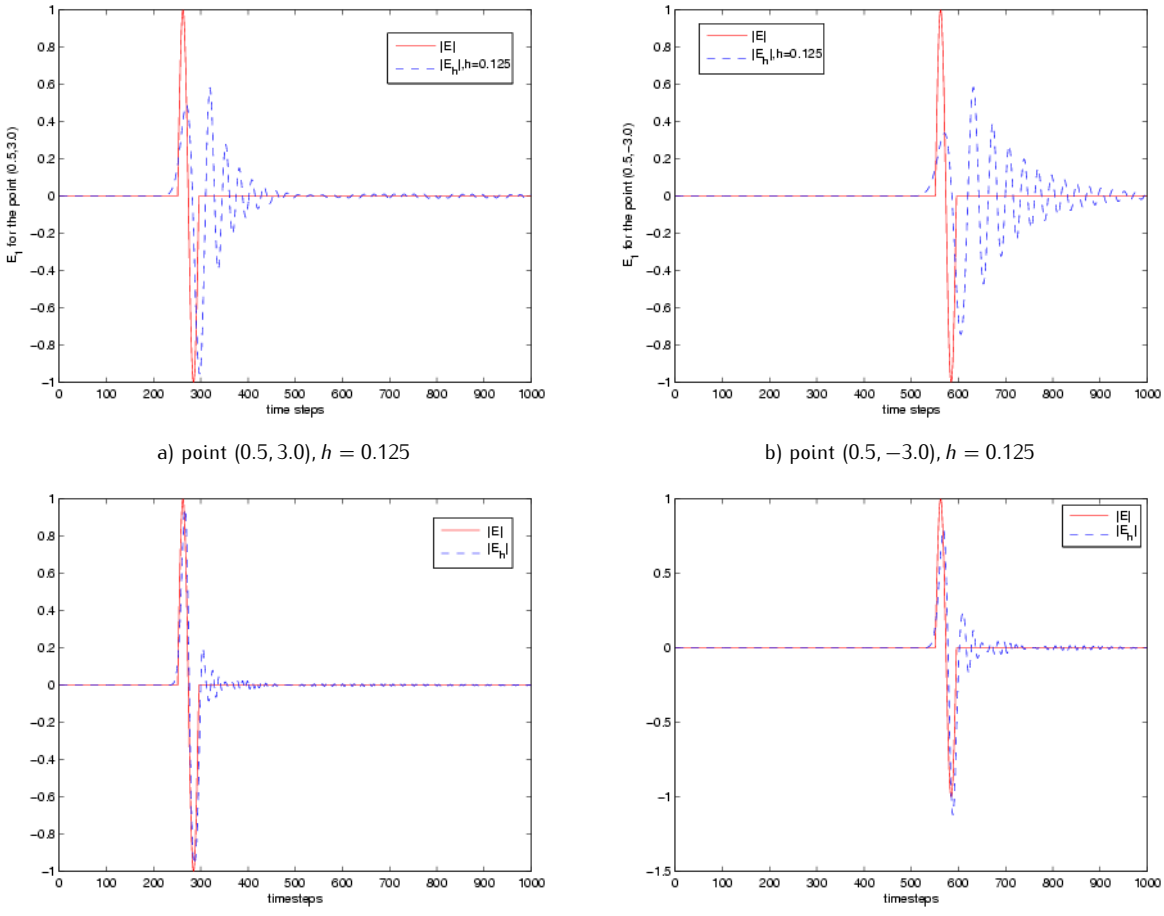

a) point $(0.5, 3.0)$, $h = 0.125$

b) point $(0.5, -3.0)$, $h = 0.125$

c) point $(0.5, 3.0)$, $h = 0.05$

d) point $(0.5, -3.0)$, $h = 0.05$

Figure 14. Test 3. Comparison of the analytic and computed solutions in the domain decomposition FEM/FDM during time $T = (0, 20)$ with $\varepsilon = \mu = 1$. We show computed domain decomposition solutions on different meshes with mesh sizes h: a) on the mesh with $h = 0.125$ at the point $(0.5, 3.0)$, which is located at the upper part of the computational domain Ω_{FEM}; b) on the mesh with $h = 0.125$ at the point $(0.5, -3.0)$, which is located at the lower of Ω_{FEM}; c) for the mesh size $h = 0.05$ at the point $(0.5, 3.0)$; d) for the mesh size $h = 0.05$ at the point $(0.5, -3.0)$.

2D case

In this test we initialize a plane wave f as in (48) that is similar to the time-resolved electromagnetic signal used in the experiments of [5, 18]. Next, we solve the problem (49)–(50) with coefficient ε in Ω_{FEM} defined as

$$\varepsilon = \begin{cases} 1 + 0.5 \sin^2 \dfrac{\pi x}{3} \cdot \sin^2 \dfrac{\pi y}{3}, & -3 \le x < 0, \quad -3 \le y < 3, \\ 1 + 0.5 \sin^2 \dfrac{\pi x}{3} \cdot \sin^2 \dfrac{\pi y}{3}, & 0 \le x \le 3, \quad 0 \le y \le 3, \\ 1 + A \sin^2 \dfrac{\pi x}{3} \cdot \sin^2 \dfrac{\pi y}{3}, & 0 \le x \le 3, \quad -3 \le y \le 0, \end{cases} \tag{53}$$

where $A = 4.0, 12.0, 26.0$, see Figure 12. Figures 17 show how the plane wave propagates in Ω, with ε in Ω_{FEM} given by (53) with $A = 4.0$, see Figure 12 a). We observe that the plane wave f is initialized at the top boundary $\partial\Omega_1$ and propagates into Ω for $t \in (0, t_1]$. First order absorbing boundary conditions [12] are used on the top $\partial\Omega_1 \times (t_1, T]$ and the bottom $\partial\Omega_2 \times (0, T]$ boundaries, and the Neumann or mirror boundary condition is used on $\partial\Omega_3 \times (0, T]$. Figures 17

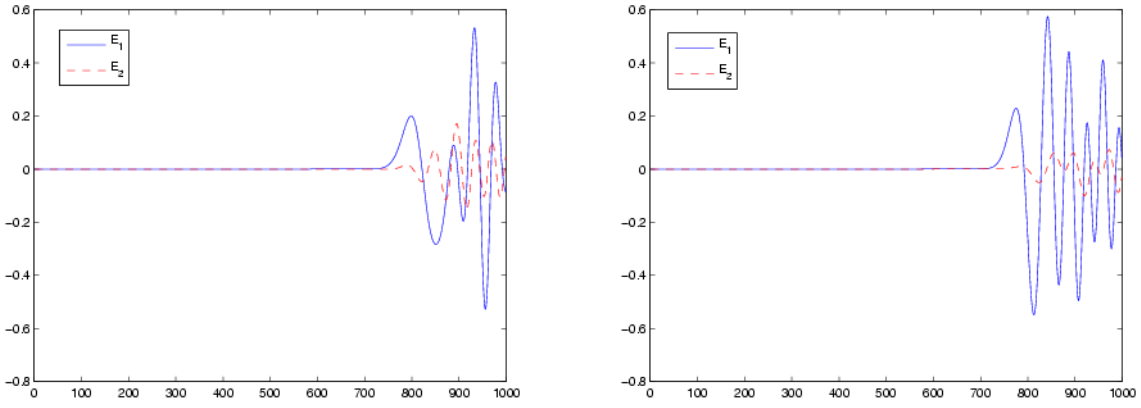

a) b)

Figure 15. Test 4. Behavior of the computed solution $E_h = (E_{1h}, E_{2h})$ during time $T = (0, 20)$ for equation (50) at different points at the FEM/FDM boundary: a) at the point $(1.0, -3.5)$; b) at the point $(1.5, -3.5)$. Here, the mesh size is $h = 0.125$ and the horizontal axis denotes the number of time steps during time $T = (0, 20)$. In this figure components of the electric field are defined as $E_1 = E_2$, $E_2 = E_1$, $E_3 = E_3$.

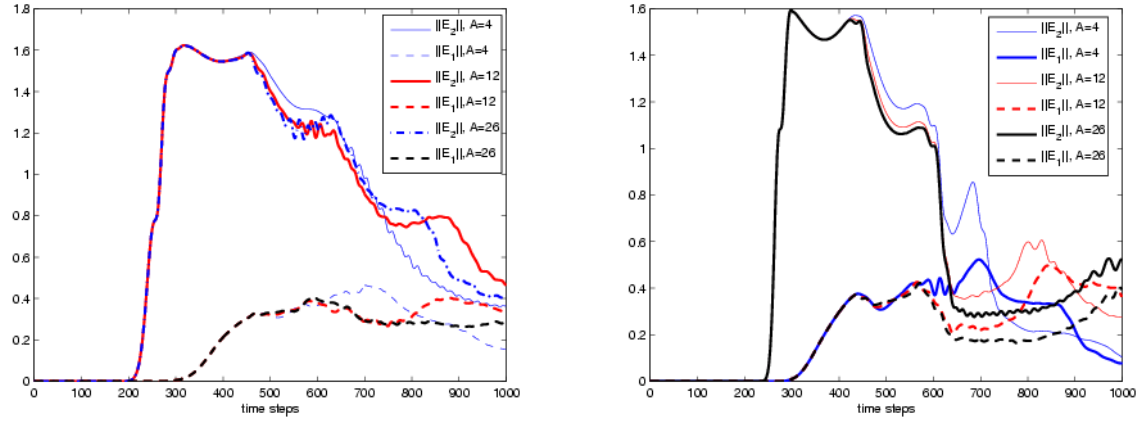

a) $h = 0.125$ b) $h = 0.05$

Figure 16. Test 4. Comparison of the computed L_2-norms for $\|E_{1h}\|$ and for $\|E_{2h}\|$ on different meshes with mesh sizes $h = 0.05$ and $h = 0.125$, respectively. L_2-norms are shown during time $T = (0, 20)$ in Ω_{FEM}. Computations are performed with different amplitudes A in the definition (53) of the coefficient $\varepsilon(x)$ inside Ω_{FEM}. Here, the horizontal axis denotes the number of time steps during time $T = (0, 20)$.

demonstrate also the continuity of the numerical solution in the domain decomposition method across the FD/FE mesh. We observe that the computed electric field $E_h = (E_{1h}, E_{2h})$ remains smooth across the FE/FD interface.

Using Figures 16–17 we can conclude that the maximum of the component E_2, where the plane wave was initialized, is about three times higher than the maximum of the component E_1 at all times. Figure 13 b) shows the comparison of the computed norms $\|E_{1h}\|$ and $\|E_{2h}\|$ during time $T = (0, 20)$ in Ω_{FEM}. In these computations we have used amplitudes $A = 4, 12, 26$ in the definition (53) of the coefficient ε inside Ω_{FEM}. From Figure 13 b), we can conclude that the computed solution E_h does not contain spurious solutions as long as values of the coefficient ε are not too big (the amplitude $A < 12$ in (53)), and the final time T is also not very large ($T < 12$).

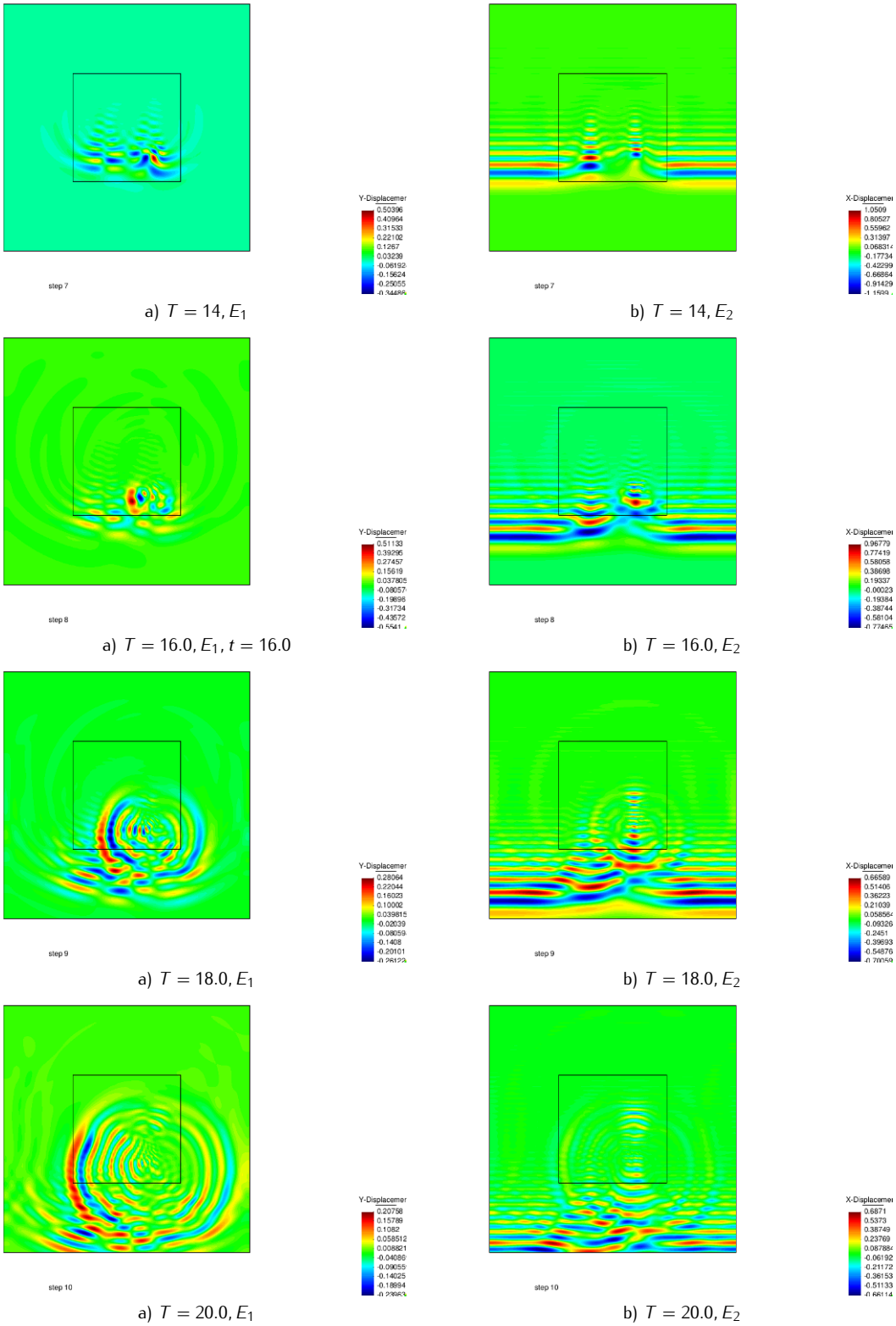

a) $T = 14, E_1$ b) $T = 14, E_2$

a) $T = 16.0, E_1, t = 16.0$ b) $T = 16.0, E_2$

a) $T = 18.0, E_1$ b) $T = 18.0, E_2$

a) $T = 20.0, E_1$ b) $T = 20.0, E_2$

Figure 17. Test 4. Computed components of the electric field $E_h = (E_{1h}, E_{2h})$ at different times in Ω using the domain decomposition FEM/FDM. The coefficient $\varepsilon(x)$ in Ω_{FEM} is defined by (53).

3D case

In this test we again initialize a plane wave f as in (48) and repeat the test of three-dimensional computations of [5, 18]. However, instead of the model of the wave equation of [5, 18] in Ω_{FEM}, now we consider the model of Maxwell's equations for the electric field E. The computational domain in the test of this section is

$$G = [-4,4]\times[-5,5]\times[-2.4,2].$$

We represent this domain as $G = \Omega_{FEM} \cup \Omega_{FDM}$, where the finite element subdomain is

$$\Omega_{FEM} = \Omega = [-3,3]\times[-3,3]\times[-2,1.4],$$

and the surrounding domain Ω_{FDM} is where we use the finite difference method. The space mesh in Ω_{FEM} consists of tetrahedra and in Ω_{FDM} of cubes with mesh size $h = 0.2$ in the overlapping regions. Thus, in Ω_{FDM} we solve problem (49) and in Ω_{FEM} we have to solve

$$\begin{aligned} \varepsilon\frac{\partial^2 E}{\partial t^2} + \nabla(\nabla\cdot E) - \nabla\cdot(\nabla E) - s\nabla(\nabla\cdot(\varepsilon E)) &= 0, \qquad \text{in} \quad \Omega_{FEM_T}, \\ E(x,0) = 0, \qquad E_t(x,0) &= 0, \qquad \text{in} \quad \Omega_{FEM}, \\ E(x,t)\restriction_{\partial\Omega_{FEM_T}} &= E(x,t)\restriction_{\partial\Omega_{\omega_{0T}}}. \end{aligned}$$

The coefficient ε inside Ω_{FEM} is defined as follows: $\varepsilon = 4$ inside a small cube with sizes $[1,2]\times[-2,-1]\times[-1,0]$, and $\epsilon = 1$ at all other points of the computational domain.

Figures 18 show reflections of all computed components of the electric field E in Ω at time moments $T = 9.42, 11.14$. These figures demonstrate also continuity of the numerical solution in the domain decomposition method across the FD/FE mesh. Figures 19 show behavior of all computed components E_{1h}, E_{2h}, E_{3h} of the electric field E at different points of the computational domain Ω_{FEM} over time. These points are located at the bottom boundary of Ω_{FEM}. Using the results of Figures 18 and 19 we make the same observation as in the two-dimensional test above: the maximum of the computed component E_{2h}, where the plane wave was initialized, is about three times larger than the maximum of other computed components E_{1h}, E_{3h} at all times. Figure 19 b) also shows a numerical comparison between all computed components E_{1h}, E_{2h}, E_{3h} of the electric field E (solid lines) versus the computed solution of the acoustic wave equation (dashed line). We observe that all reflections corresponding to the solution of the acoustic wave equation approximate the reflections from the computed component E_{2h} of the electric field very well. Thus, we can conclude that all meaningful reflections from the coefficient $\varepsilon(x)$ are from the component E_2, while reflections from the other components of the electric field E_1, E_3 are negligible compared with reflections from the component E_2. This fact explains why in the experiments of [5, 18] it was only possible to measure the single time-resolved signal and why the other two components in our 3D test of [5, 18] could not be measured — reflections from these remaining components were negligible. Because of the above observations as well as results of Figure 19 b), we have approximated in [5, 18] our model problem of Maxwell's system with a single wave equation.

8. Conclusion

The modified stabilized domain decomposition FEM/FDM of this paper can be applied to the solutions of the coefficient inverse problems, for example, to reconstruct the dielectric permittivity function $\varepsilon(x)$ of the medium under investigation with the condition that the electric permeability $\mu(x) = 1$ in the whole domain. Applications of the proposed modified domain decomposition FEM/FDM for solutions of CIPs are broad, from airport security to the imaging of land mines. In all such applications we need to reconstruct the relative dielectric constant ε_r of explosives, which are 3–5 times higher than ones of regular materials, see http://www.clippercontrols.com.

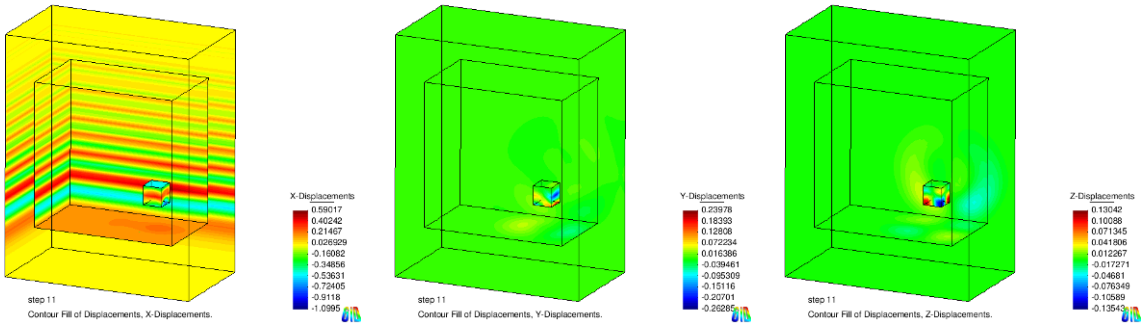

a) E_{2h}, $T = 9.42$ b) E_{1h}, $T = 9.42$ c) E_{3h}, $T = 9.42$

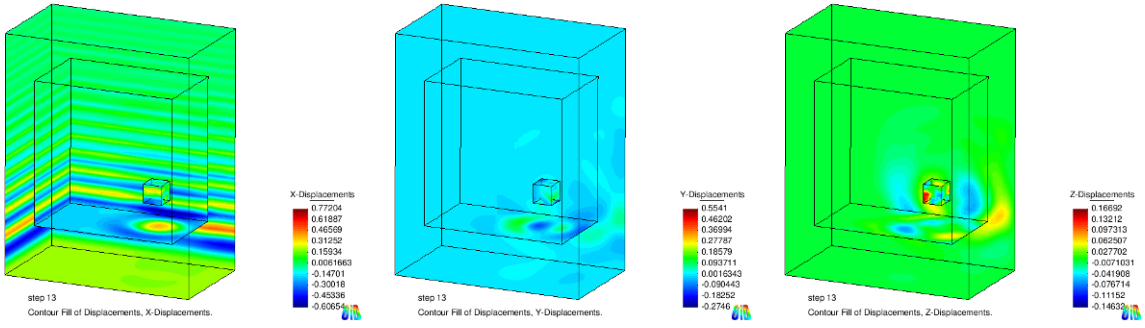

a) E_{2h}, $T = 11.14$ b) E_{1h}, $T = 11.14$ c) E_{3h}, $T = 11.14$

Figure 18. Test 4. Computed components of the electric field $E_h = (E_{1h}, E_{2h}, E_{3h})$ in Ω using the domain decomposition FEM/FDM at different times.

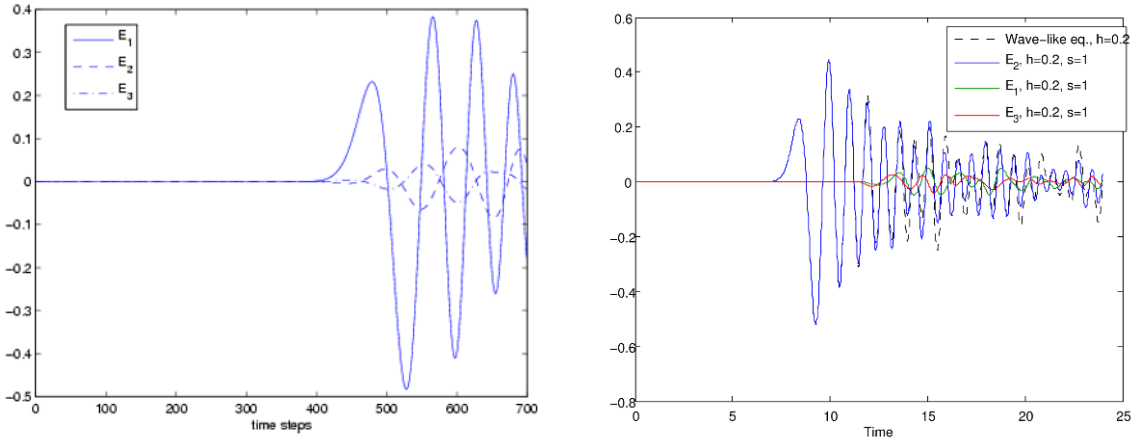

a) point $(0.0, -3.0, 0.0)$ b) point $(1.5, -3.0, 0.0)$

Figure 19. Test 4. Behavior of the computed electric field $E_h = (E_{1h}, E_{2h}, E_{3h})$ at different points of the computational domain Ω_{FEM}: a) during time $T = (0, 12)$ (in this figure components of electric field are defined as $E_1 = E_2, E_2 = E_1, E_3 = E_3$); b) during time $T = (0, 24)$. In a) the horizontal axis denotes the number of time steps in time.

Acknowledgements

This work was supported by the Swedish Research Council, Swedish Foundation for Strategic Research (SSF) through the Gothenburg Mathematical Modeling Center (GMMC) and by the Swedish Institute, Visby program. The author acknowledges also Mohammad Asadzadeh for useful discussions and suggestions.

References

[1] Assous F., Degond P., Heintze E., Raviart P.-A., Serge J., On a finite-element method for solving the three-dimensional Maxwell equations, J. Comput. Phys., 1993, 109(2), 222–237
[2] Beilina L., Grote M.J., Adaptive hybrid finite element/difference method for Maxwell's equations, TWMS J. Pure Appl. Math., 2010, 1(2), 176–197
[3] Beilina L., Johnson C., A posteriori error estimation in computational inverse scattering, Math. Models Methods Appl. Sci., 2005, 15(1), 23–37
[4] Beilina L., Johnsson C., Hybrid FEM/FDM method for an inverse scattering problem, In: Numerical Mathematics and Advanced Applications, Ischia, July, 2001, Springer, Milan, 2003, 545–556
[5] Beilina L., Klibanov M.V., Reconstruction of dielectrics from experimental data via a hybrid globally convergent/adaptive inverse algorithm, Inverse Problems, 2010, 26(12), #125009
[6] Beilina L., Samuelsson K., Åhlander K., Efficiency of a hybrid method for the wave equation, In: Finite Element Methods, Jyväskylä, 2000, GAKUTO Internat. Ser. Math. Sci. Appl., 15, Gakkōtosho, Tokyo, 2001, 9–21
[7] Brenner S.C., Scott L.R., The Mathematical Theory of Finite Element Methods, Texts Appl. Math., 15, Springer, New York, 1994
[8] Budak B.M., Samarskii A.A., Tikhonov A.N., A Collection of Problems in Mathematical Physics, Dover Phoenix Ed., Dover, Mineola, 1988
[9] Cangellaris A.C., Wright D.B., Analysis of the numerical error caused by the stair-stepped approximation of a conducting boundary in FDTD simulations of electromagnetic phenomena, IEEE Trans. Antennas and Propagation, 1991, 39(10), 1518–1525
[10] Edelvik F., Ledfelt G., Explicit hybrid time domain solver for the Maxwell equations in 3D, J. Sci. Comput., 2000, 15(1), 61–78
[11] Elmkies A., Joly P., Éléments finis d'arête et condensation de masse pour les équations de Maxwell: le cas 2D, C. R. Acad. Sci. Paris Sér. I Math., 1997, 324(11), 1287–1293
[12] Engquist B., Majda A., Absorbing boundary conditions for the numerical simulation of waves, Math. Comp., 1977, 31(139), 629–651
[13] Hughes T.J.R., The Finite Element Method, Prentice Hall, Englewood Cliffs, 1987
[14] Jiang B., The Least-Squares Finite Element Method, Scientific Computation, Springer, Berlin–Heidelberg, 1998
[15] Jiang B.-N., Wu J. Povinelli L.A., The origin of spurious solutions in computational electromagnetics, J. Comput. Phys., 1996, 125(1), 104–123
[16] Jin J., The Finite Element Method in Electromagnetics, John Wiley & Sons, New York, 1993
[17] Joly P., Variational Methods for Time-Dependent Wave Propagation Problems, In: Topics in Computational Wave Propagation, Lect. Notes Comput. Sci. Eng., 31, Springer, Berlin, 2003, 201–264
[18] Klibanov M.V., Fiddy M.A., Beilina L., Pantong N., Schenk J., Picosecond scale experimental verification of a globally convergent algorithm for a coefficient inverse problem, Inverse Problems, 2010, 26(4), #045003
[19] Ladyzhenskaya O.A., The Boundary Value Problems of Mathematical Physics, Appl. Math. Sci., 49, Springer, New York, 1985
[20] Monk P.B., Finite Element Methods for Maxwell's Equations, Oxford University Press, New York, 2003
[21] Monk P.B., Parrott A.K., A dispersion analysis of finite element methods for Maxwell's equations, SIAM J. Sci. Comput., 1994, 15(4), 916–937
[22] Munz C.-D., Omnes P., Schneider R., Sonnendrücker E., VoßU., Divergence correction techniques for Maxwell solvers based on a hyperbolic model, J. Comput. Phys., 2000, 161(2), 484–511

[23] Paulsen K.D., Lynch D.R., Elimination of vector parasites in finite element Maxwell solutions, IEEE Trans. Microwave Theory Tech., 1991, 39(3), 395–404
[24] Perugia I., Schötzau D., The *hp*-local discontinuous Galerkin method for low-frequency time-harmonic Maxwell equations, Math. Comp., 2002, 72(243), 1179–1214
[25] Rylander T., Bondeson A., Stable FEM-FDTD hybrid method for Maxwell's equations, Comput. Phys. Comm., 2000, 125(1-3), 75–82
[26] Rylander T., Bondeson A., Stability of explicit-implicit hybrid time-stepping schemes for Maxwell's equations, J. Comput. Phys., 2002, 179(2), 426–438
[27] Yee K.S., Numerical solution of initial boundary value problems involving Maxwell's equations in isotropic media, IEEE Trans. Antennas and Propagation, 1966, 14(3), 302–307